Galactic chemical evolution in hierarchical formation models - I. Early-type galaxies in the local Universe

Arrigoni, Matías; Trager, Scott C.; Somerville, Rachel S.; Gibson, Brad K.

Published in:
Monthly Notices of the Royal Astronomical Society

DOI:
10.1111/j.1365-2966.2009.15924.x

Publication date:
2010

Monthly Notices
of the
ROYAL ASTRONOMICAL SOCIETY

Mon. Not. R. Astron. Soc. **402,** 173–190 (2010) doi:10.1111/j.1365-2966.2009.15924.x

Galactic chemical evolution in hierarchical formation models – I. Early-type galaxies in the local Universe

Matías Arrigoni,[1⋆] Scott C. Trager,[1] Rachel S. Somerville[2,3] and Brad K. Gibson[4]

[1]*Kapteyn Astronomical Institute, University of Groningen, Postbus 800, NL-9700 AV Groningen, the Netherlands*
[2]*Space Telescope Science Institute, 3700 San Martin Drive, Baltimore, MD 21218, USA*
[3]*Department of Physics and Astronomy, Johns Hopkins University, Baltimore, MD 21218, USA*
[4]*Jeremiah Horrocks Institute for Astrophysics & Supercomputing, University of Central Lancashire, Preston PR1 2HE*

Accepted 2009 October 21. Received 2009 October 21; in original form 2009 May 6

ABSTRACT

We study the metallicities and abundance ratios of early-type galaxies in cosmological semi-analytic models (SAMs) within the hierarchical galaxy formation paradigm. To achieve this we implemented a detailed galactic chemical evolution model and can now predict abundances of individual elements for the galaxies in the semi-analytic simulations. This is the first time a SAM with feedback from active galactic nuclei has included a chemical evolution prescription that relaxes the instantaneous recycling approximation. We find that the new models are able to reproduce the observed mass–metallicity ($M_\star$–[Z/H]) relation and, for the first time in a SAM, we reproduce the observed positive slope of the mass–abundance ratio ($M_\star$–[α/Fe]) relation. Our results indicate that in order to simultaneously match these observations of early-type galaxies, the use of both a very mildly top-heavy initial mass function (i.e. with a slope of $x = 1.15$ as opposed to a standard $x = 1.3$), and a lower fraction of binaries that explode as Type Ia supernovae (SNe Ia) appears to be required. We also examine the rate of SN explosions in the simulated galaxies. In early-type (non-star-forming) galaxies, our predictions are also consistent with the observed SNe rates. However, in star-forming galaxies, a higher fraction of SN Ia binaries than in our preferred model is required to match the data. If, however, we deviate from the classical model and introduce a population of SNe Ia with very short delay times, our models simultaneously produce a good match to the observed metallicities, abundance ratios and SN rates.

Key words: galaxies: abundances – galaxies: evolution – galaxies: formation.

1 INTRODUCTION

The chemical properties and abundance ratios of galaxies provide important constraints on their formation histories. Galactic chemical evolution (GCE) has been modelled in detail in the monolithic collapse scenario (e.g. Matteucci & Greggio 1986; François et al. 2004; Pipino & Matteucci 2004; Pipino & Matteucci 2006; Romano et al. 2005). These models have successfully described the abundance distributions in our Galaxy and other spiral discs, as well as the trends of metallicity and abundance ratios observed in early-type galaxies. In the last three decades, however, the paradigm of hierarchical assembly in a cold dark matter (CDM) cosmology has revised the picture of how structure in the Universe forms and evolves. In this scenario, galaxies form when gas radiatively cools and condenses inside dark matter (DM) haloes, which themselves follow dissipationless gravitational collapse (White & Rees 1978; White & Frenk 1991). The CDM picture has been successful at predicting many observed properties of galaxies, though many potential problems and open questions remain. It is therefore interesting to see whether chemical evolution models, when implemented within this modern cosmological context, are able to correctly predict the observed chemical properties of galaxies.

The semi-analytic approach provides a cosmological framework in which to study galaxy formation and chemical evolution in different environments, by following the merger history of DM haloes and the relevant physical processes such as gas cooling, star formation and feedback (e.g. White & Frenk 1991; Kauffmann, White & Guiderdoni 1993; Cole et al. 1994; Cole et al. 2000; Somerville & Primack 1999; Somerville, Primack & Faber 2001; Hatton et al. 2003). A major challenge for models of galaxy formation within the CDM picture arises from the mismatch between the *shape* of the mass function of the DM haloes and that of the baryonic condensations that we call galaxies (White & Frenk 1991; Kauffmann et al. 1993; Somerville & Primack 1999; Benson et al. 2003). The CDM theory predicts a steeper slope for low-mass haloes, and a

⋆E-mail: arrigoni@astro.rug.nl
There is an Erratum to this article at doi:10.1111/j.1365-2966.2012.20697.x.

more gradual drop-off in the abundance of high-mass haloes than is seen in luminous galaxies, implying that the formation of stars must be inefficient in both low-mass and high-mass haloes (Moster et al. 2009). However, the inclusion of physically motivated, if still ad hoc, feedback processes in the semi-analytic models (SAMs) can cure these discrepancies. The faint end of the luminosity function can be matched with a combination of supernova (SN) feedback and suppression of gas cooling in low-mass haloes as a result of a photoionizing background. At the bright end, heating by giant radio jets powered by accreting black holes has become a favoured mechanism for preventing overcooling and quenching star formation in massive haloes (Bower et al. 2006; Croton et al. 2006; Somerville et al. 2008b, hereafter S08). This latest generation of SAMs is successful at reproducing many properties of galaxies at the present and at high redshift, for example, the luminosity and stellar mass function of galaxies, colour–magnitude or star formation rate (SFR) versus stellar mass distributions, relative numbers of early- and late-type galaxies, gas fractions and size distributions of spiral galaxies and the global star formation history (SFH; e.g. Bower et al. 2006; Cattaneo et al. 2006; Croton et al. 2006; De Lucia et al. 2006; S08; Fontanot et al. 2009; Kimm et al. 2009, to name just a few).

The modelling of chemical enrichment of the galaxies and intergalactic (and intracluster) gas, however, has not been thoroughly developed in SAMs, and to date most SAMs have only used the instantaneous recycling approximation [in essence only considering enrichment by Type II supernovae (SNe II)] and trace only the total metal content. There are, however, a few models that have included a more refined treatment of the chemical enrichment. Thomas (1999) and Thomas & Kauffmann (1999) were the first to include enrichment by Type Ia supernovae (SNe Ia) in models with cosmologically motivated SFHs. However, rather than implementing the chemical evolution self-consistently within a SAM, they made use of SFHs from the SAM and assumed a closed-box model (no gas inflows or outflows) for the chemical evolution. They calculated the evolution of [Fe/H] and [Mg/Fe] and found a decreasing trend of [Mg/Fe] with increasing galaxy luminosity, in stark disagreement with observations (e.g. Worthey, Faber & Gonzalez 1992; Trager et al. 2000a, b; Thomas et al. 2005).

The first SAM to self-consistently track a variety of elements due to enrichment by SNe Ia and SNe II was that of Nagashima et al. (2005a,b). Among other things, they adopted a bimodal initial mass function (IMF) described by a standard IMF for normal quiescent star formation in discs and an extremely flat 'top-heavy' IMF during merger-driven starbursts. This model was motivated by the difficulty that SAMs with a standard IMF experienced in reproducing the observed population of very luminous sub-mm galaxies at high redshift (Baugh et al. 2005). However, the notion that early-type galaxies form their stars with an IMF flatter than standard is not new and has been proposed many times in the past as a plausible explanation for the abundance patterns in early-type galaxies and in the intracluster medium (ICM) of galaxy clusters (e.g. Worthey, Faber & Gonzalez 1992; Matteucci & Gibson 1995; Gibson & Matteucci 1997; Thomas, Greggio & Bender 1999). The predictions of the Nagashima et al. model were in good agreement with the abundances of the ICM of galaxy clusters, matching the trend of individual elements (O, Fe, Mg, Si) and abundance ratios with ICM temperature. However, the same model failed to reproduce the trend of [α/Fe] in early-type galaxies, where they found that the abundance ratio decreases with increasing galactic velocity dispersion, again in clear contradiction with observations. Very recently, Pipino et al. (2009) have coupled GCE to the GalICS SAM (Hatton et al. 2003), and obtained results similar to those of Nagashima et al. (2005b).

In a simple closed-box picture, it is well known that galaxies with short star formation time-scales are expected to have enhanced [α/Fe] ratios (because their enrichment is dominated by α-rich Type II SNe), while galaxies with extended SFHs tend to have lower [α/Fe] (e.g. Worthey et al. 1992; Thomas 1999; Thomas et al. 1999; Thomas & Kauffmann 1999; Trager et al. 2000b), because of the additional Fe contributed by delayed Type Ia enrichment. Therefore a possible interpretation of the difficulties that CDM-based galaxy formation models have experienced in reproducing the positive trend between mass, luminosity or velocity dispersion and abundance ratio is related to the issue of so-called 'downsizing'. This refers to the variety of observational evidence that high-mass galaxies formed their stars early and over short time-scales, while low-mass galaxies have more extended SFHs (see Fontanot et al. 2009, for a summary). Before the inclusion of active galactic nuclei (AGN) feedback or some other mechanism that quenches star formation in massive haloes, CDM-based galaxy formation models predicted the opposite trend (massive galaxies continued to accrete gas and form stars until the present day, leading to extended SFHs). It has been demonstrated that including radio-mode AGN feedback in SAMs leads to a 'downsizing' trend for star formation that is at least qualitatively in better agreement with observations (De Lucia et al. 2006; S08; Fontanot et al. 2009; Trager & Somerville 2009, hereafter TS09). Therefore we expect that the new models might do better at reproducing the trend of [α/Fe] with mass as the more massive galaxies will have shorter star formation time-scales.

Clearly, observations of chemical abundances and abundance ratios in various phases [stellar, interstellar medium (ISM), ICM] offer the opportunity to obtain strong constraints on galaxy formation histories and the physics that shapes them. However, in order to take advantage of these observations, it is necessary to implement detailed modelling of chemical evolution into a full modern SAM that includes the relevant physical processes (e.g. triggered star formation and morphological transformation of galaxies via mergers, the growth of supermassive black holes and AGN feedback). In this work we incorporate detailed chemical evolution into the semi-analytic galaxy formation model of S08, taking into account enrichment by SNe Ia, SNe II and long-lived stars, and abandoning the instantaneous recycling approximation by considering the finite lifetimes of stars of all masses. The delay in the metal enrichment by SNe Ia is calculated self-consistently according to the lifetimes of the progenitor stars. This is, to our knowledge, the first time that detailed chemical evolution has been included in a SAM with AGN feedback (both radio-mode heating and AGN-driven winds). The base model includes gas inflows due to radiative cooling of gas and outflows due to SN and AGN-driven winds. We compute the abundances of many α and Fe-peak elements for early-type galaxies of different masses, exploring different IMF slopes and values for the fraction of binaries that yield a SN Ia event, and compare these with observations of abundances and abundance ratios for a sample of local early-type galaxies. We also calculate SNe rates using both the classical Greggio & Renzini (1983) approach for SN Ia and the more recent delay time distribution (DTD) formalism (Greggio 2005). Another improvement in the present work is our use of re-calibrated estimates for chemical abundances obtained from line strengths in early-type galaxies (see Appendix B for details).

The outline of the paper is as follows. In Section 2 we give an overview of the main ingredients of the SAM. In Section 3 we describe in detail the adopted treatment for the chemical evolution. In Section 4 we present our predictions and compare them with

observations. In Section 5 we summarize our findings and present our conclusions. Two appendices describe the detailed implementation of the chemical evolution model and the data used in this paper.

2 THE SEMI-ANALYTIC MODEL

In this section we summarize the basic ingredients of the SAM used to model the formation and evolution of galaxies. These include the growth of structure of the DM component in a hierarchical clustering framework, radiative cooling of gas, star formation, SN feedback, AGN feedback, galaxy merging within DM haloes, metal enrichment of the ISM and ICM and the evolution of stellar populations. The reader is referred to Somerville & Primack (1999), Somerville et al. (2001) and especially S08 for a comprehensive and detailed description of the different prescriptions used in this SAM. In what follows we briefly sketch the modelling of the most important physical processes.

2.1 Dark matter merger trees and galaxy merging

The merging histories (or merger trees) of DM haloes are constructed based on the extended Press–Schechter formalism using the method described in Somerville & Kolatt (1999), with improvements described in S08. Each branch in the tree represents a merger event, and, in order to make the process finite, the trees are followed down to a minimum progenitor mass of $10^{10}\,\mathrm{M}_{\odot}$.

Whenever DM haloes merge, the central galaxy of the largest progenitor becomes the new central galaxy, and all others become 'satellites'. Satellite galaxies may eventually merge with the central galaxy due to dynamical friction. To model the time-scale of the merger process we use a variant of the Chandrasekhar formula from Boylan-Kolchin, Ma & Quataert (2008). Tidal stripping and destruction of satellites are also included as described in S08.

2.2 Gas cooling, star formation and supernova feedback

Before the universe is re-ionized, each halo contains a mass of hot gas equal to the universal baryon fraction times the virial mass of the halo. After re-ionization, the photoionizing background can suppress the collapse of gas into low-mass haloes. We use the results of Gnedin (2000) and Kravtsov, Gnedin & Klypin (2004) to model the fraction of baryons that can collapse into haloes of a given mass after re-ionization.

When a DM halo collapses, or merges with a larger halo, the gas within it is shock heated to the virial temperature of the halo, and gradually radiates and cools at a rate given by the cooling function. To calculate this function we use the metallicity-dependent radiative cooling curves of Sutherland & Dopita (1993). A detailed description of how the cooling process is modelled can be found in S08. The rate at which gas can cool is given by

$$\dot{m}_{\mathrm{cool}} = \frac{1}{2} m_{\mathrm{hot}} \frac{r_{\mathrm{cool}}}{r_{\mathrm{vir}}} \frac{1}{t_{\mathrm{cool}}}, \tag{1}$$

where m_{hot} is the mass of the hot halo gas, r_{vir} is the virial radius of the DM halo, r_{cool} is the radius within which all of the gas can cool in a time t_{cool}, which itself depends on density, metallicity and temperature. In our models, we assume that the cold gas is accreted only by the central galaxy of the halo, but in reality satellite galaxies should also receive some measure of new cold gas. This aspect of the modelling should be improved (cf. Pipino et al. 2009) and for the present study we restrict our analysis to *only* the central galaxy of each halo, except when otherwise stated.

When the gas cools we assume that it settles into a rotationally supported disc. The radial sizes of the discs are calculated according to the results described in Somerville et al. (2008a), and agree well with observed disc sizes to $z \sim 2$.

We model the SFR in quiescent discs with a recipe based on the empirical Schmidt–Kennicutt law (Kennicutt 1989):

$$\dot{m}_{\star} = \frac{2\pi A_K \Sigma_0^{N_K} r_{\mathrm{gas}}^2}{N_K^2} \times \left[1 - \left(1 + \frac{N_K r_{\mathrm{crit}}}{r_{\mathrm{gas}}}\right) \exp(-N_K r_{\mathrm{crit}}/r_{\mathrm{gas}})\right], \tag{2}$$

where $\dot{m}_{\star}$ is the SFR, $\Sigma_0 \equiv m_{\mathrm{cold}}/(2\pi\, r_{\mathrm{gas}}^2)$ is the average surface density of the cold gas, r_{gas} is the scalelength of the gaseous disc (assumed to be an exponential disc with its scalelength proportional to that of the stellar disc), r_{crit} is the radius at which the gas reaches the critical surface density threshold for star formation (Σ_{crit}) and A_K and N_K are the normalisation and slope of the SFR law. We adopt the values $A_K = 8.35 \times 10^{-5}$, $N_K = 1.4$ and $\Sigma_{\mathrm{crit}} = 6\,\mathrm{M}_{\odot}\,\mathrm{pc}^{-2}$, as in S08.

Galaxy mergers in the SAM trigger enhanced episodes of star formation. The burst is modelled by two parameters, the time-scale and the efficiency of the burst. The time-scale is a function of the virial velocity of the progenitor galaxies, the equation of state of the gas, the cold gas fraction in the discs and the redshift (Robertson et al. 2006). The efficiency, which is defined as the fraction of the cold gas reservoir (of both galaxies) that is turned into stars during the burst, is assumed to be a power-law function of the mass ratio of the merging galaxies, and the exponent of the power law depends on the galaxy morphology (Cox et al. 2008). The collisional starburst occurs in addition to any ongoing 'normal' quiescent star formation, which continues uninterrupted through the merger but is usually insignificant in comparison to the burst. Any new stars formed during the burst are always placed in the bulge component of the resulting galaxy.

As SNe occur, they inject energy into the ISM and reheat the cold gas, which is then expelled from the disc and incorporated into the hot halo gas where it can cool again. The rate of reheating by SNe is given by

$$\dot{m}_{\mathrm{rh}} = \epsilon_0^{\mathrm{SN}} \left(\frac{V_{\mathrm{disc}}}{200\,\mathrm{km\,s^{-1}}}\right)^{-\alpha_{\mathrm{rh}}} \dot{m}_{\star}, \tag{3}$$

where ϵ_0^{SN} and α_{rh} are free parameters. The circular velocity of the disc V_{disc} is taken to be equal to the maximum rotational velocity of the DM halo. Some fraction of the reheated gas can also be ejected from the halo entirely into the diffuse intergalactic medium (IGM). This fraction is described by

$$f_{\mathrm{eject}}(V_{\mathrm{vir}}) = \left[1.0 + (V_{\mathrm{vir}}/V_{\mathrm{eject}})^{\alpha_{\mathrm{eject}}}\right]^{-1}, \tag{4}$$

where $\alpha_{\mathrm{eject}} = 6$ and V_{eject} is a free parameter in the range $\simeq$ 100–150 $\mathrm{km\,s^{-1}}$. This ejected gas is allowed to recollapse into the halo at later times and once again becomes available for cooling.

2.3 Formation of spheroids

In most SAMs each merger is classified as 'major' or 'minor' depending on whether the ratio of the smaller to the larger galaxies' baryonic masses is greater than or less than the parameter $f_{\mathrm{ellip}} \sim 0.25$, respectively. The usual assumption is then that, in a major merger, the bulge and disc stars of both progenitor galaxies, as well

as the stars formed in the merger driven starburst (see below), are transferred to the bulge component of the resulting galaxy. In a minor merger, all the pre-existing stars of the smaller galaxy end up in the disc of the post-merger galaxy, and all the newly formed stars are placed in bulge. We follow a similar practise here, but instead of using a sharp threshold to define major or minor mergers, we use a more gradual transition function. In detail, when two galaxies with bulge masses B_1 and B_2, and disc masses D_1 and D_2 merge, the resulting galaxy has a bulge mass $B_{\rm new} = B_1 + B_2 + f_{\rm sph}(D_1 + D_2)$ and a disc mass $D_{\rm new} = (1 - f_{\rm sph})(D_1 + D_2)$. The value $f_{\rm sph}$ is a continuous function of the *total* mass ratio (baryons and DM) in the *central* parts of the galaxy (see S08).

2.4 Black hole growth and AGN feedback

The models of S08 also track the growth of supermassive black holes and the energy they release. Each top-level DM halo is seeded with a $\sim$100 $M_\odot$ black hole, and these black holes are able to grow via two different accretion modes. The first accretion mode is fuelled by cold gas that is driven into the nucleus of the galaxy by mergers. This mode is radiatively efficient, and the accretion rates are close to the Eddington limit. Because this accretion mode is associated with optically bright classical quasars and AGN, it is referred to as 'bright mode' or 'quasar mode' accretion. The second mode is fuelled by hot gas in a quasi-hydrostatic halo, and the accretion rate is modelled via the Bondi–Hoyle approximation. Accretion rates in this mode are significantly sub-Eddington ($\sim 10^{-4}$ to 10^{-3} times the Eddington rate) and the accretion is assumed to be radiatively inefficient. This mode is, however, associated with the production of giant radio jets, and is therefore referred to as the 'radio mode'.

Energy released during 'bright mode' activity can couple with the cold gas in the galaxy via radiation pressure, driving galactic scale winds that can eject cold gas from the galaxy. The mass outflow rate due to the AGN-driven wind is modelled by the following formula:

$$\dot{m}_{\rm agn} = \epsilon_{\rm wind}\eta_{\rm rad}\frac{c}{V_{\rm esc}}\dot{m}_{\rm acc}, \quad (5)$$

where $\epsilon_{\rm wind}$ is the effective coupling efficiency, $V_{\rm esc}$ is the escape velocity of the galaxy and $\dot{m}_{\rm acc}$ is the accretion rate of mass on to the black hole.

The radio jets produced by 'radio mode' activity are assumed to inject thermal energy into the hot halo gas, partly or completely offsetting the cooling flow. This process is responsible for quenching the star formation in massive galaxies (which contain massive black holes) and solves the 'overcooling problem' that plagued CDM-based galaxy formation models for many years.

2.5 Stellar population synthesis and dust

In order to compare the luminosities and colours of the galaxies in the simulations with real observations, we convolve the star formation and chemical enrichment history of each galaxy with the multimetallicity simple stellar population (SSP) models of Bruzual & Charlot (2003). We use the models based on the Padova 1994 (Bertelli et al. 1994) isochrones with a Chabrier (2001) IMF.

We also model the effects of dust extinction. Based on the model of Charlot & Fall (2000), we consider extinction due to two components, one due to the diffuse dust in the disc and another associated with the dense 'birth clouds' surrounding young star forming regions. The V band, face-on extinction optical depth of the diffuse dust is given by

$$\tau_{V,0} \propto \tau_{\rm dust,0} Z_{\rm cold} m_{\rm cold}/(r_{\rm gas})^2, \quad (6)$$

where $\tau_{\rm dust,0}$ is a free parameter, $Z_{\rm cold}$ is the metallicity of the cold gas, $m_{\rm cold}$ is the mass of the cold gas in the disc and $r_{\rm gas}$ is the radius of the cold gas disc. To compute the actual extinction we assign each galaxy a random inclination and use a standard 'slab' model. Additionally, stars younger than 10^7 yr are enshrouded in a cloud of dust with optical depth $\tau_{{\rm BC},V} = \mu_{\rm BC}\,\tau_{V,0}$, where $\mu_{\rm BC} = 3$. Finally, to extend the extinction correction to other wavebands, we assume a Galactic attenuation curve (Cardelli, Clayton & Mathis 1989) for the diffuse dust component and a power-law extinction curve $A_\lambda \propto (\lambda/5500\text{Å})^n$, with $n = 0.7$, for the birth clouds.

2.6 Cosmological and galaxy formation parameters

We adopt a flat ΛCDM cosmology with $\Omega_0 = 0.2383$, $\Omega_\Lambda = 0.7617$, $h \equiv H_0/(100\,{\rm km\,s^{-1}\,Mpc^{-1}}) = 0.732$, $\sigma_8 = 0.761$ and a cosmic baryon fraction of $f_{\rm b} = 0.1746$, following the results of Spergel et al. (2007). We adopt these parameters for consistency with the published models of S08, but find that we obtain nearly identical results with the updated values of the cosmological parameters from Komatsu et al. (2009).

We leave the values of the free parameters associated with the galaxy formation models fixed to the fiducial values given in S08. These values were chosen by requiring that the models reproduced key observations of nearby galaxies, such as the $z \sim 0$ stellar mass function, and gas fractions and SFRs as a function of stellar mass. These models have also been shown to produce reasonable agreement with observed local galaxy colour distributions in Kimm et al. (2009), and with observed stellar mass functions and SFRs at high redshift ($0 < z < 4$; Fontanot et al. 2009). In Section 4.1 we check that our new models, with the updated treatment of chemical evolution modelling, still reproduce the key observational quantities with the same values of the free parameters.

3 GALACTIC CHEMICAL EVOLUTION

In S08, the production of metals was tracked using a simple approach commonly adopted in SAMs (see e.g. Somerville & Primack 1999; Cole et al. 2000; De Lucia, Kauffmann & White 2004; Kang et al. 2005). In a given time-step, when we create a parcel of new stars d m_*, we also create a mass of metals d $M_Z = y\,{\rm d}m_*$, which we assume to be instantaneously mixed with the cold gas in the disc. The yield y is assumed to be constant, and is treated as a free parameter.[1] We track the mean metallicity of the cold gas $Z_{\rm cold}$, and when we create a new parcel of stars they are assumed to have the same metallicity as the mean metallicity of the cold gas in that time-step. SN feedback ejects metals from the disc, along with cold gas. These metals are either mixed with the hot gas in the halo, or ejected from the halo into the 'diffuse' IGM, in the same proportion as the reheated cold gas. The ejected metals in the 'diffuse gas' reservoir are also re-accreted into the halo in the same manner as the gas.

In the present study, we discard the instantaneous recycling approximation and allow the ISM to be enriched by the products of SNe Ia and SNe II on their own time-scales. Consequently, we now track individual elements, and not just the total metal content. The integrated ejecta of each element is not a free parameter, but instead

[1] The yield parameter y should not take arbitrary values since it is constrained by the IMF and the theory of stellar nucleosynthesis (albeit subject to the uncertainties in both). However, it is treated in most SAMs as a free parameter.

is calculated according to theoretical yields and the SFHs provided by the SAM. In the next subsection we describe the implementation of the new chemical evolution model in detail.

3.1 Basic equations of the GCE

For the purposes of tracing the enrichment of the ISM, we still model our galaxies as a single zone with instantaneous mixing of gas. We assume that newly produced metals are deposited into the cold gas, and may subsequently be ejected from the galaxy and mixed with the hot halo gas (or ejected from the halo altogether) according to the feedback model described above. The metallicity of each new batch of stars equals that of the cold gas at the moment of formation. In this context, the evolution of the abundance of metals in the cold gas is given by

$$\dot{G}_Z(t) = -\psi(t)Z(t) + e_Z(t) + [\dot{G}_Z(t)]_{\rm inflow} - [\dot{G}_Z(t)]_{\rm outflow}, \tag{7}$$

where $G(t)$ is the total mass of gas and $Z(t)$ is the mass-weighted metal abundance, $G_Z(t) = G(t)Z(t)$ is the mass of gas in the form of metals, $\psi(t)$ is the SFR, $\psi(t)Z(t)$ represents the rate at which metals are depleted from the ISM by star formation, $e_Z(t)$ is the rate of ejecta of enriched material by dying stars (integrated over stellar mass) and the last two terms represent the infall of cooled halo gas into the galaxy and the outflow of reheated gas from the galaxy. Here we refer generally to 'metals' for simplicity, but in fact we apply this equation to each individual element by considering the abundance Z_i of a given element i instead of the total metallicity Z. For comprehensive reviews of equation (7), we direct the reader to Tinsley (1980) and Pagel (1997). The modelling of the SFR, the inflow rate (cooling flows) and the outflow rate (SNe and AGN-driven galactic winds) has already been sketched in the previous section. The different prescriptions shown before relate to the terms in equation (7) in the following way:

$$\begin{aligned} \psi(t)Z(t) &= \dot{m}_\star Z_{\rm c}, \\ \left[\dot{G}_Z(t)\right]_{\rm inflow} &= \dot{m}_{\rm cool} Z_{\rm h}, \\ \left[\dot{G}_Z(t)\right]_{\rm outflow} &= (\dot{m}_{\rm rh} + \dot{m}_{\rm agn}) Z_{\rm c}, \end{aligned} \tag{8}$$

where $Z_{\rm c}$ and $Z_{\rm h}$ are the abundances of the cold ISM gas and the hot halo gas, respectively.

In most SAMs previous to this work, chemical evolution was traced in a very simple manner by assuming a constant 'effective yield', or mean mass of metals produced per mass of stars, and the value of this effective yield was treated as a free parameter. In the models presented here, we have implemented detailed calculations for the production of heavy elements and the chemical enrichment of the ISM (the second term in equation 7) in a similar fashion to the models of Matteucci & Gibson (1995), Timmes, Woosley & Weaver (1995) and Pipino & Matteucci (2004). In this framework, not only do we trace the evolution of the total metallicity, but we also track the distinct elements as well. At this moment we can follow the evolution of the abundances of 19 different elements, but here we will only discuss α-elements and Fe. By α-elements we mean the composite abundance of N, Na, Ne, Mg, Si and S. At any given time, the rate at which an element i restored into the ISM is calculated according to the following formula:

$$\begin{aligned} e_{Z_i} = & \int_{M_{\rm L}}^{M_{{\rm B}_m}} \psi(t-\tau_M) Q_{mi}(t-\tau_M)\phi(M)\,{\rm d}M \\ & + A \int_{M_{{\rm B}_m}}^{M_{{\rm B}_M}} \phi(M_{\rm B}) \\ & \times \left[\int_{\mu_{\rm min}}^{0.5} f(\mu)\psi(t-\tau_{M_2}) Q_{mi}(t-\tau_{M_2})\,{\rm d}\mu\right] {\rm d}M_{\rm B} \\ & + (1-A) \int_{M_{{\rm B}_m}}^{M_{{\rm B}_M}} \psi(t-\tau_M) Q_{mi}(t-\tau_M)\phi(M)\,{\rm d}M \\ & + \int_{M_{{\rm B}_M}}^{M_{\rm U}} \psi(t-\tau_M) Q_{mi}(t-\tau_M)\phi(M)\,{\rm d}M, \end{aligned} \tag{9}$$

where $M_{\rm L}$ and $M_{\rm U}$ are the lower and upper masses of stars formed, $\psi(t)$ is the SFR as before, $\phi(M)$ is the IMF, $f(\mu)$ is the distribution function for the mass of the secondary star in a binary pair ($\mu = M_2/M_{\rm B}$), τ_M is the lifetime of a star of mass M and $Q_{mi}(t)$ represent the fractional mass of an element i restored by a star of mass M in the form of both newly synthesized and unprocessed material. Although not explicitly dependent on time, the quantities Q_{mi} depend on metallicity, which of course evolves in time.

Each of the integrals in equation (9) represents the contribution to the enrichment by stars in different mass ranges. The first integral indicates the contribution of single stars with masses between $M_{\rm L} = 0.8\,{\rm M}_\odot$ (the minimum mass which can restore gas to the ISM within a Hubble time) and $M_{{\rm B}_m} = 3\,{\rm M}_\odot$ (the minimum mass of a binary system which can give rise to a SNe Ia event). These stars eject their chemical by-products through stellar winds and end their lives as white dwarfs. The second integral refers to the contribution from SNe Ia, assuming that these events originate from C–O white dwarfs in binary systems exploding by C-deflagration after reaching the Chandrasekhar mass. This implies a maximum primary mass of $8\,{\rm M}_\odot$, and therefore $M_{{\rm B}_M} = 16\,{\rm M}_\odot$ and $\mu_{\rm min} = \max[(M_{\rm L}/M_{\rm B}), (M_{\rm B} - 8\,{\rm M}_\odot)/M_{\rm B}]$. The parameter A represents the fraction of binary systems with total mass in the appropriate range that actually give rise to a SNe Ia event. In essence, A is a free parameter. Chemical evolution models of the Milky Way constrain the value of this parameter to around $A \sim 0.04$–0.05 by ensuring compatibility with the observed present-day rate of SNe I and SNe II in our Galaxy (François et al. 2004). However, this value results in an unacceptably high abundance of Fe and Fe-peak elements in our models. Therefore, we allow this parameter to take different values (0.015, 0.02, 0.03, 0.05) and constrain it a posteriori by comparison with abundance ratios and SNe rates (see also the discussion in de Plaa et al. 2007). The distribution function of the secondary mass fraction is assumed to follow the law

$$f(\mu) = 2^{1+\gamma}(1+\gamma)\mu^\gamma, \tag{10}$$

with $\gamma = 2$. A complete description of all the quantities involved in the computation of the SNe I rate can be found in Greggio & Renzini (1983) and Matteucci & Greggio (1986). Note that in this scheme, it is the mass of the secondary star (M_2) that sets the clock for the explosion. This *implies* a specific DTD for the explosions that may not represent reality (see Section 4.2). The third integral represents the mass restored by stars in the mass range 3–16 $\rm M_\odot$ which are either single, or, if binaries, do not produce a SN I event. These stars end their lives as white dwarfs ($M < 8\,{\rm M}_\odot$) or as SNe II ($M > 8\,{\rm M}_\odot$). Finally, the last term represents the contribution of short-lived massive stars ($M > 16\,{\rm M}_\odot$) that explode as SNe II. The fact that we take into account the lifetimes of the stars implicitly involves a time delay for the different enrichment modes (AGB

stellar winds, SNe I and SNe II) since the integrands in equation (9) are by definition zero whenever $t < \tau_M$.

Before applying the GCE to the SAM, we tested the chemical evolution code separately. We ran simulations using only the chemical evolution algorithm and compared the results with simple models with analytic solutions, i.e. a closed box with either constant and continuous star formation or a single initial burst of star formation. We also compared our results with the output from other well-tested models, namely that of Fenner & Gibson (2003). Only after achieving satisfactory agreement in these tests did we proceed to implement the chemical evolution into the SAM.

3.2 Ingredients of the GCE

In the previous section, we introduced several fundamental quantities that determine the chemical enrichment of a galaxy's cold gas reservoir and described them in a qualitative manner. In what follows, we will point the reader to the different studies that quantify the ingredients of this model, and the values adopted for the simulations presented in the next section. We discuss the implementation in Appendix A.

3.2.1 Initial mass function

The stellar IMF that we use is based on the parametrization of Chabrier (2003):

$$\phi(m) = \begin{cases} \mathcal{A}\, \mathrm{e}^{-(\log m - \log m_\mathrm{c})^2/2\sigma^2} & \text{if } m < 1\,\mathrm{M}_\odot, \\ \mathcal{B}\, m^{-x} & \text{if } m > 1\,\mathrm{M}_\odot, \end{cases} \tag{11}$$

where in the standard Chabrier IMF, $x = 1.3$, $\sigma = 0.69$, $m_\mathrm{c} = 0.079\,\mathrm{M}_\odot$ and the proportionality constants take the values $\mathcal{A} = 0.9098$ and $\mathcal{B} = 0.2539$ after normalization in the mass interval 0.1–40 $\mathrm{M}_\odot$. This IMF differs somewhat from the standard power laws of Salpeter (1955) and Kroupa, Tout & Gilmore (1993) often used in the literature. The reason for this choice is consistency with the stellar population synthesis models that are used to predict magnitudes and colours in the simulations, since those models use the Chabrier IMF (Bruzual & Charlot 2003). Note that this expression is for the IMF by mass.

We show below that the results with this IMF were not entirely satisfactory. We therefore explored different slopes ($x = 1.2$, 1.1, 1.0) and upper mass limits ($M_\mathrm{U} = 60$, 100, 120 $\mathrm{M}_\odot$). The values of the normalization constants $\mathcal{A}$ and $\mathcal{B}$ for different values of x and M_U are computed by requiring that

$$\int_{M_\mathrm{L}}^{M_\mathrm{U}} \phi(m)\,\mathrm{d}m = 1. \tag{12}$$

We note that these alternate values for the slope are within the observational uncertainties (Chabrier 2003), and certainly do not represent a radical departure from the observed local IMF.

3.2.2 Stellar lifetimes

The adopted relation between the evolutionary lifetimes and the stellar mass is that of Padova tracks for solar metallicity (Bertelli et al. 1994). In principle the lifetimes depend not only on mass but also on metallicity. Nevertheless the difference in stellar ages for different metal abundances is smaller than the age binning in the grid that stores the SFH of the galaxies in our simulations (see Appendix A).

3.2.3 Stellar yields

Stellar yields are the amount of material that a star can produce and eject into the ISM in the form of a given element, and are clearly one of the most important ingredients in any chemical evolution model. These yields are the quantities Q_{mi} in the equations above. In this work we adopt different nucleosynthesis prescriptions for stars in the different mass ranges.

Low- and intermediate-mass stars ($0.8 < M/\mathrm{M}_\odot < 8$) produce He, C, N and heavy s-process elements,[2] which they eject during the formation of a planetary nebulae. The yields that we adopt are from Karakas & Lattanzio (2007, hereafter KL07).

Massive stars ($M > 8\,\mathrm{M}_\odot$) produce mainly α-elements (O, Na, Ne, Mg, Si, S, Ca), some Fe-peak elements, light s-process elements and r-process elements. They explode as core-collapse SNe II. We adopt the yields from Woosley & Weaver (1995, hereafter WW95). Note that the upper mass limit in this study is 40 $\mathrm{M}_\odot$.

SNe Ia are assumed to be C–O white dwarfs in binary systems, exploding by C-deflagration after reaching the Chandrasekhar mass via accretion of material from the companion star. They mainly produce Fe and Fe-peak elements. The yields we adopt are from Nomoto et al. (1997, hereafter N97), model W7. When calculating the contribution of SNe Ia, we assume that the primary star also enriches the medium as a normal AGB prior to the SN event.

Except for the SN Ia yields, which are given only for solar metallicity, we use metallicity-dependent yields, namely those tabulated for $Z = 0.0002$, 0.004, 0.02, interpolating when necessary but never extrapolating. Whenever the metallicity falls below or above the limiting values, we use the yields corresponding to the minimum or maximum Z, respectively.

Note that unlike in some recent studies of GCE (François et al. 2004; Pipino & Matteucci 2004, 2006; Nagashima et al. 2005a,b) we do not alter the yields in any way in our standard model. We want to see if we can fit the data with as few degrees of freedom as possible.

3.3 Delay time distribution formulation for SNe Ia

As mentioned before, and shown in Section 4.2, the SN Ia model described in the previous subsection does not seem to be the best representation of this phenomenon. In order to test other models, we implemented the DTD formalism developed by Greggio (2005). In this scenario, the SN Ia rate is described by

$$R_{Ia}(t) = k_\alpha \int_{\tau_i}^{\min(t,\tau_x)} A(t-\tau)\psi(t-\tau)\mathrm{DTD}(\tau)\,\mathrm{d}\tau, \tag{13}$$

where $\psi(t)$ is the SFR, τ_i is the minimum delay time for the SN Ia events which we assume to be equal to the lifetime of an 8 $\mathrm{M}_\odot$ star, τ_x is the maximum delay and equal to the lifetime of a 0.8 $\mathrm{M}_\odot$ star and k_α is the number of stars per unit mass in a stellar generation defined by

$$k_\alpha = \int_{M_\mathrm{L}}^{M_\mathrm{U}} \phi(m) m^{-1}\,\mathrm{d}m. \tag{14}$$

Finally, $A(t-\tau)$ is the fraction of binary systems which give rise to SNe Ia and may, in principle, evolve in time, but here we will assume it to be constant. It should be noted that in this case, $A(t-\tau)$ is the fraction relative to the full mass range defined by the

[2] At this point we do not trace s-process or r-process elements, but they will be included in future versions of the code.

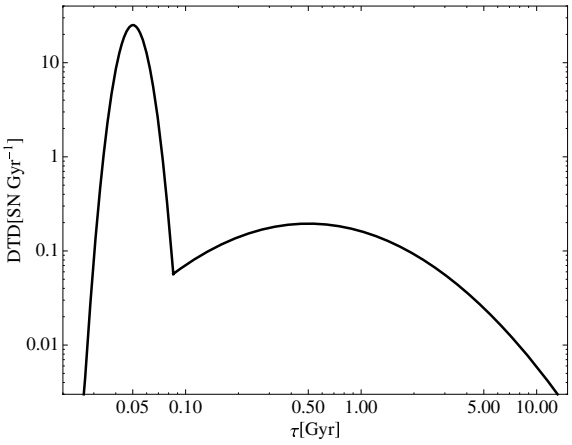

Figure 1. The normalized DTD proposed by Mannucci et al. (2006), and adopted in this work.

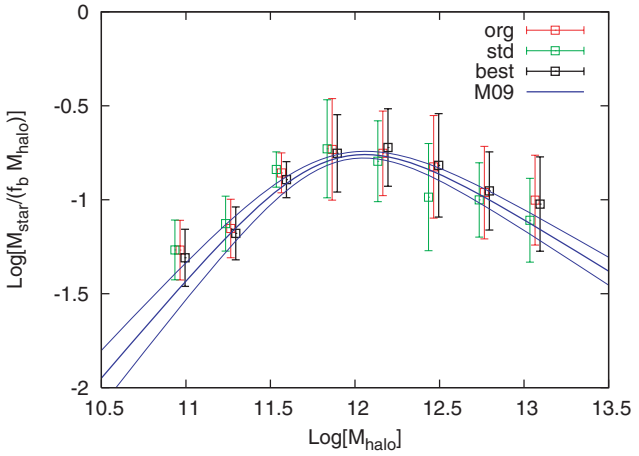

Figure 2. The fraction of baryons in the form of stars as a function of halo mass for model galaxies in the SAM+GCE with the *best-fitting* parameters ($x = 1.1$ and $A = 0.015$, black squares), with *standard* parameters ($x = 1.3$ and $A = 0.05$, green squares) and in the *original* SAM without GCE (red squares). The blue lines mark the empirical relation, and 1σ uncertainties, derived by Moster et al. (2009).

IMF ($M_{\rm L}$–$M_{\rm U}$) and not only the mass range 3–16 $M_\odot$ as before. To ease the comparison with the previous model we will define $A(t - \tau) = A\, f_{3-\!-16}$, where $f_{3-\!-16}$ is the fraction of stars in the 3–16 $M_\odot$ mass range (defined by the IMF) and A has the usual meaning.

This formulation allows for different SNe Ia models depending on the DTD(τ) used. In particular we have chosen the distribution favoured by Mannucci, Della Valle & Panagia (2006), and parametrized it in similar way as Matteucci et al. (2006):

$$\log \mathrm{DTD}(\tau) = \begin{cases} 1.4 - 50(\log\tau + 1.3)^2 & \text{if } \tau < \tau_{\rm o}, \\ -0.71 - 0.9(\log\tau + 0.3)^2 & \text{if } \tau > \tau_{\rm o}, \end{cases} \quad (15)$$

where delay time τ is in Gyr, $\tau_{\rm o} = 0.0851$ Gyr, and the distribution function is normalized so that

$$\int_{\tau_i}^{\tau_x} \mathrm{DTD}(\tau)\,\mathrm{d}\tau = 1. \quad (16)$$

In Fig. 1 we show the behaviour of the implemented DTD. Note that for a single burst of star formation, about half of all SN Ia explosions occur within the first 100 Myr.

4 RESULTS

In this section we present the first results of our model and compare them with stellar population studies of a variety of early-type galaxies in the local Universe. For this purpose, we ran simulations for a grid of DM haloes of different masses, ranging from 10^{11} to 10^{13} $M_\odot$, using both the original (instantaneous recycling) and new (full GCE) version of the semi-analytic code. As mentioned before, we limit our analysis to the central galaxies of each DM halo. We selected early-type galaxies from our simulations according to the ratio of their bulge-to-total luminosity in the B band; namely, we consider a galaxy to be an early type when this ratio is larger than 0.4047 (Simien & de Vaucouleurs 1986). This selection encompasses both elliptical and S0 galaxies. Unless otherwise noted, the model results presented in this section are always for central early-type galaxies. We begin with a comparison of the results of our new model with those of the S08 SAM. We then proceed to compare the predictions of the new model with observations. For the purpose of this comparison, we will only show model galaxies with masses above 10^9 $M_\odot$ since the formation history for galaxies below this mass cannot be accurately resolved given the mass resolution of the DM trees (see Section 2.1).

4.1 Impact of the new GCE modelling in galaxy observables

The new chemical evolution modelling affects the physics in the SAM in at least three ways: changing the metallicity of the hot gas changes the cooling rates; changing the metallicity of the cold gas changes the amount of dust, and therefore observed colours and magnitudes and the metallicities themselves and their evolution change as well. The original version of the S08 SAM did very well at reproducing several key properties of galaxies and it is important to verify that this is still the case after implementing the detailed chemical evolution model. For this purpose we will compare simulations with three different 'flavours' for the models: the *original* SAM from S08, a SAM+GCE with *standard* parameters (i.e. $x = 1.3$ and $A = 0.05$) and a SAM+GCE with parameters that best fit (*best-fitting*) the abundance ratios and metallicities of observed galaxies ($x = 1.1$ and $A = 0.015$, see Section 4.2).

A fundamental feature that any good galaxy formation model must reproduce is the luminosity function or stellar mass function of galaxies. Given the distribution function of DM haloes and subhaloes predicted by CDM, the relationship between stellar mass and halo mass implies a specific stellar mass function. The required stellar mass to halo mass relationship, in the form of the fraction of baryons in the halo that are converted to stars in a galaxy, has been derived by Wang et al. (2006) and Moster et al. (2009). In Fig. 2 we show the stellar mass fraction as a function of halo mass for the SAM with and without GCE and compared with the empirical relation obtained by Moster et al. (2009). The agreement between all 'flavours' of the models (S08, standard parameters, best-fitting) and the observations is excellent. This implies that the stellar mass function in our new models will be nearly identical to that presented in S08, which was shown to agree well with observations.

In Fig. 3 we show the average SFHs of our model early-type galaxies, for galaxies with different present-day stellar masses. As pointed out in previous studies (see e.g. De Lucia et al. 2006; S08; TS09), SAMs with AGN feedback do qualitatively reproduce a downsizing-like trend (i.e. the higher mass galaxies have shorter star formation time-scales and less extended SFH). This is still true in our new models.

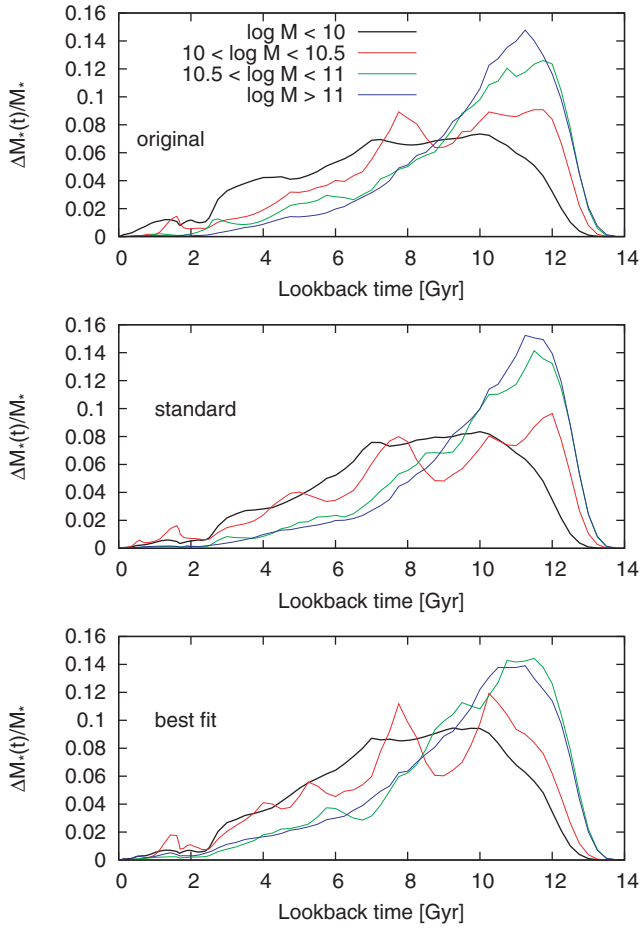

Figure 3. Smoothed average SFHs for model early-type galaxies in (from bottom to top) the SAM+GCE with the *best-fitting* parameters ($x = 1.1$ and $A = 0.015$), with *standard* parameters ($x = 1.3$ and $A = 0.05$) and in the *original* SAM without GCE, binned by the stellar mass of the galaxy at $z = 0$.

Another very important observational quantity to reproduce is the colour–magnitude diagram (CMD) of galaxies. In Fig. 4 we show magnitudes and colours of early-type galaxies in the SAM with and without GCE. Here there is one caveat regarding the calculation of the galaxy luminosities. The stellar population models that we use to predict the colours and magnitudes (Bruzual & Charlot 2003) use a fixed standard Chabrier IMF, while we allow the slope of this IMF to change when calculating the chemical evolution. Although this is not self-consistent, such a minor change in the IMF parameters should not significantly affect the predicted colours or magnitudes since the early-type galaxies studied here are dominated by old populations for which high-mass stars are of little importance (C. Conroy, private communication). We divide the CMD into red and blue regions using the magnitude-dependent cut of Baldry et al. (2004). The galaxies form two clear groups: the majority in a bright red sequence and a few in a fainter blue cloud. The 'original' and 'best-fitting' models agree quite well with the observed CMD, while the luminous galaxies in the 'standard model' are slightly too blue.

In the previous version of the SAM, the fraction of cold gas relative to stars in galactic discs at the present time was used to calibrate the models by comparison with the observational estimates of Bell et al. (2003) for morphologically late-type galaxies (see fig. 5 in S08). This property is well reproduced by all test cases after implementing the GCE. Here we also compare the gas fraction of

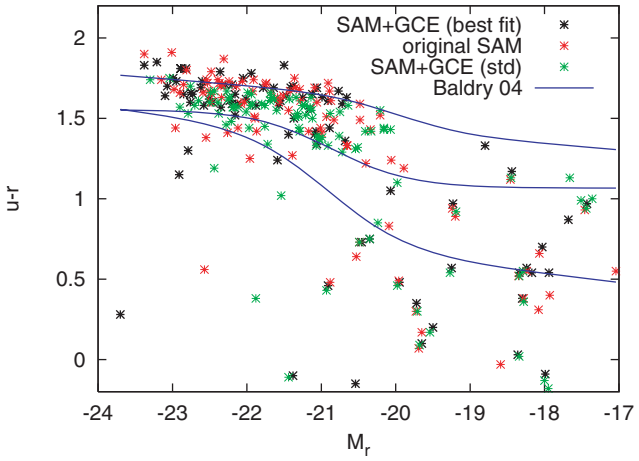

Figure 4. CMD for model early-type galaxies in the SAM+GCE with the *best-fitting* parameters ($x = 1.1$ and $A = 0.015$, black stars), with *standard* parameters ($x = 1.3$ and $A = 0.05$, green stars) and in the *original* SAM without GCE (red stars). The blue lines mark, from top to bottom, the locus of the red sequence, the green valley and the blue cloud from Baldry et al. (2004).

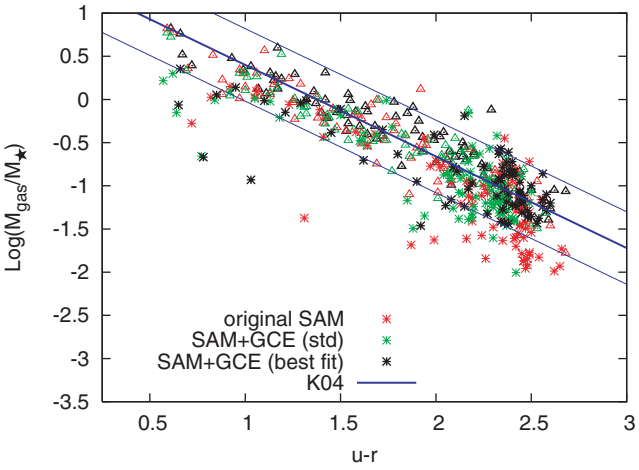

Figure 5. The gas fraction for model galaxies in the SAM+GCE with the best-fitting parameters ($x = 1.1$ and $A = 0.015$, black symbols), with standard parameters ($x = 1.3$ and $A = 0.05$, green symbols) and in the original SAM without GCE (red symbols) as a function of $u - r$ colour. Stars and triangles depict early-type and disc galaxies, respectively. The thick blue line marks the median of the sample from Kannappan (2004), and the thin lines mark the 1σ deviation.

our galaxies, both early type and discs, with those from Kannappan (2004) as a function of $u - r$ colour, as shown in Fig. 5. The agreement in the slope, scatter and zero-point of the relation is quite good for all models, especially when the new model of GCE is included.

The first evidence for the mass–metallicity relation can be seen when looking at the metallicity distribution function of galaxies of different masses, which we show in Fig. 6 for our three test cases. All of the models agree qualitatively, showing an increasing mean of the distribution as the mass range increases. At a given mass, however, the distributions for the best-fitting model are shifted to higher metallicities since galaxies in this simulation are more metal rich (see below).

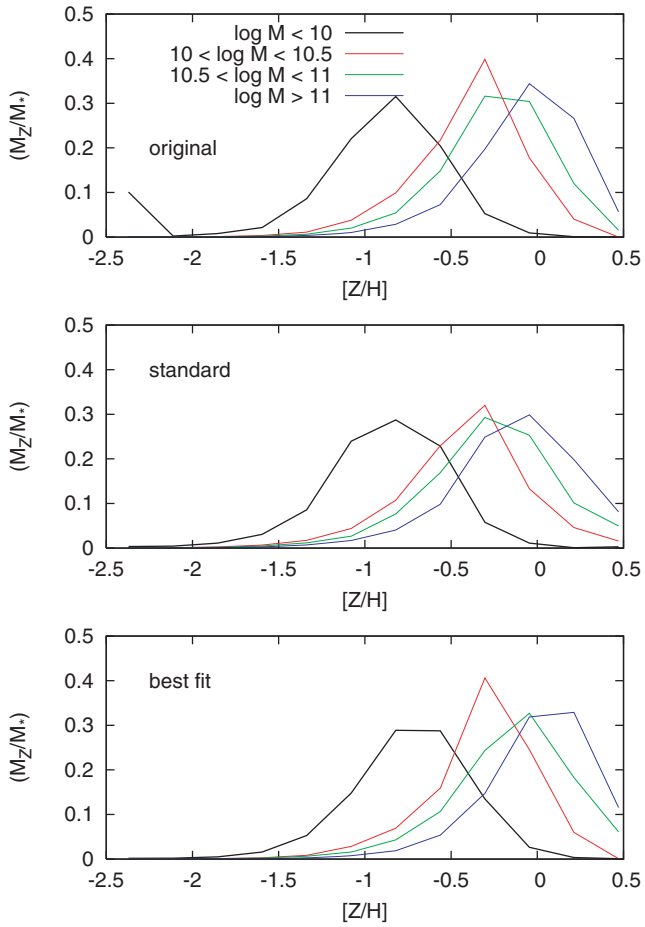

Figure 6. Average metallicity distributions for model early-type galaxies in (from bottom to top) the SAM+GCE with the best-fitting parameters ($x = 1.1$ and $A = 0.015$), with standard parameters ($x = 1.3$ and $A = 0.05$) and in the SAM without GCE, binned by stellar mass.

Summarizing, we have seen that including a detailed chemical evolution model in the SAM has a minor effect on the predicted formation histories and present-day properties of galaxies, and therefore does not require a recalibration of the free parameters of the model. In the next subsection we will investigate the predicted metallicities and abundances, which are indeed affected by the GCE.

4.2 Chemistry of early-type galaxies

The main effect of the new treatment of chemical evolution is reflected in the metallicity and abundance ratios of the galaxies. Most SAMs reproduce fairly well the mass–metallicity relation of galaxies (with effective yield treated as a free parameter), but to date they have been unsuccessful in fitting the slope of the mass–[α/Fe] relation (e.g. Nagashima et al. 2005b; Pipino et al. 2009). This is the main challenge that we address in this study.

The galaxy sample used for comparison is that described in Trager et al. (2000a). This sample has been re-analysed using the updated stellar population synthesis method presented in Trager, Faber & Dressler (2008), which is sensitive to age, metallicity and abundance ratios. In the current study, we use models based on the Bruzual & Charlot (2003) models with index variations due to abundance ratios taken from Lee et al. (2009). Inferred stellar population parameters are tabulated in Appendix B. When making the comparisons, we use

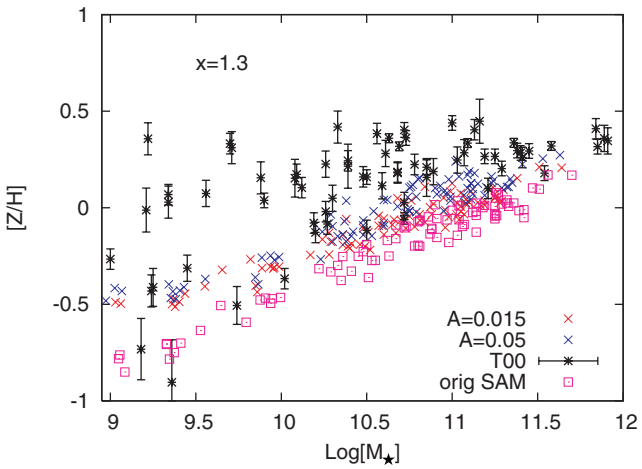

Figure 7. The relationship between metallicity and stellar mass for the galaxies in our simulations and in the observational sample of T00. Symbols – pink squares: original SAM; red crosses: SAM+GCE with $x = 1.3$ and $A = 0.015$; blue crosses: SAM+GCE with $x = 1.3$ and $A = 0.05$; black stars with error bars: galaxies from Trager et al. (2000a), re-analysed as described in the text. Note the poor agreement of the model galaxies with the observations in all cases.

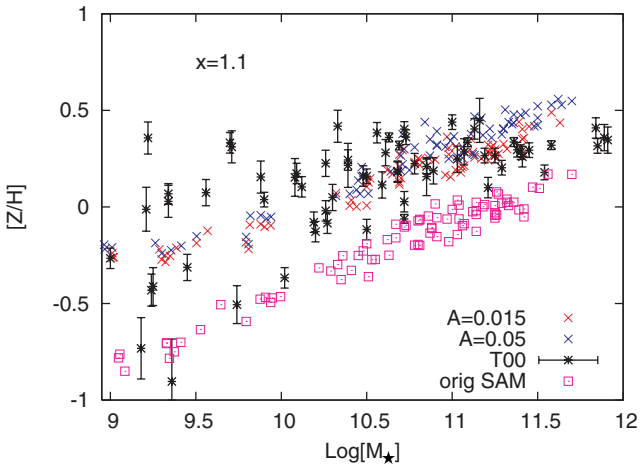

Figure 8. As in Fig. 7, except with a shallower high-mass slope for the IMF ($x = 1.1$) used in the SAM+GCE. Note the significantly better agreement of the model galaxies with the observations.

the stellar mass of the simulated galaxies and the inferred dynamical mass of the observed ones. This should not introduce a significant bias since the dynamical mass is a good tracer of the stellar mass within one effective radius for most early-type galaxies (Cappellari et al. 2006). The abundances presented here were normalized to the solar values from Grevesse, Noels & Sauval (1996). We have also computed the present epoch SNe Ia and II rates for our galaxies and compared them with the results of Mannucci et al. (2005) and Sullivan et al. (2006).

4.2.1 Dependence on IMF slope and SN Ia fraction

In Figs 7 and 8 we show the relation between total metallicity ([*Z*/H]) and stellar mass ($M_\star$). From these figures, we see that in the 'old' SAMs, galaxies tended to be too metal poor compared to the observations (as seen in TS09), and implementing the detailed chemical evolution with the standard IMF improves the results only

slightly. We explore the parameter space of the GCE equations to see if it is possible to improve the agreement with the observations. Specifically, the parameters allowed to vary are the fraction of binaries that give rise to SNe Ia (A in equation 9), the slope of the IMF above $1\,M_\odot$ (x in equation 11) and the upper mass limit of the IMF (M_U in equation 9). However, we will only show the results for $M_U = 40\,M_\odot$ for the following reason. Given that our chosen SN II yields (WW95) are only tabulated up to that value, we are forced to assume that the yields relative to the initial mass remain constant and equal to those of a $40\,M_\odot$ star for stars above this value when running simulations with higher upper mass limits. This proves to be an unreliable assumption, as reflected for example in the non-monotonic behaviour of the [α/Fe] ratio as a function of the stellar mass of our galaxies, in serious disagreement with observations. Other properties, such as the SNe Ia rate, are not significantly affected by this parameter, as expected.

We also note that, even though we have varied the slope of the IMF, the SN feedback efficiency remains the same because the prescription for the SN feedback energetics and the SN chemical enrichment are decoupled; the SN feedback efficiency is set manually as a free parameter (see equation 3), independent of the IMF. In this sense, the model is not entirely self-consistent. However, this choice makes it easier to interpret the effect of changing the IMF in the models.

We now compare the predictions for the observed galaxy sample, the original SAM and the new SAM with GCE with a standard Chabrier IMF, a shallower IMF ($x = 1.1$) and two choices of the parameter A (0.015 and 0.05). The use of a shallower IMF results in an upward shift in the zero-point of the mass–metallicity relation, bringing it into much better agreement with the observations. This increase in metallicity with a shallower IMF is expected since more massive stars are produced and therefore the gas is enriched more efficiently. The metallicities of the model galaxies show almost no dependence on the parameter A, which is not surprising since this parameter mainly controls the ratio of SNe Ia to SNe type II, affecting abundance ratios but not the overall metallicity (in essence the production of α-elements and Fe-peak elements compensate for one another).

A primary advantage of our new model is that we can now calculate abundance ratios for our galaxies, which gives us yet another property to compare with observations and set further constraints on the models. This is shown in Figs 9 and 10, where we plot the [α/Fe] ratio against stellar mass for the same parameter choices as before. For the simulated galaxies, we consider the abundance of α-elements to be the composite abundance of N, Na, Ne, Mg, Si and S (cf. Trager et al. 2000a). If we assume a value of the parameter $A \sim 0.05$ commonly used in the literature, the abundance ratios are far too low. The overall values of [α/Fe] can be raised by decreasing the value of A (i.e. producing fewer SNe Ia and consequently less iron). However, even with this decreased A and the standard IMF, we see that the relation is too flat or even has a slightly negative slope, and for the galaxies at the high-mass end the [α/Fe] ratio is insufficiently enhanced. On the other hand, a shallower IMF, combined with a lower value of A, produces model galaxies in far better agreement with observations. The flatter IMF increases the slope of the relation while a low A brings up the zero-point. Moreover, it is interesting to note that lowering A also increases the slope (at any fixed IMF). This small steepening of the [α/Fe]–mass relation is due to the metallicity dependence of the yields, since the higher the initial metallicity, the higher the [α/Fe] in the yields. A lower fraction of SNe Ia (and consequently more type II) implies a slightly faster overall enrichment, and therefore galaxies spend more time

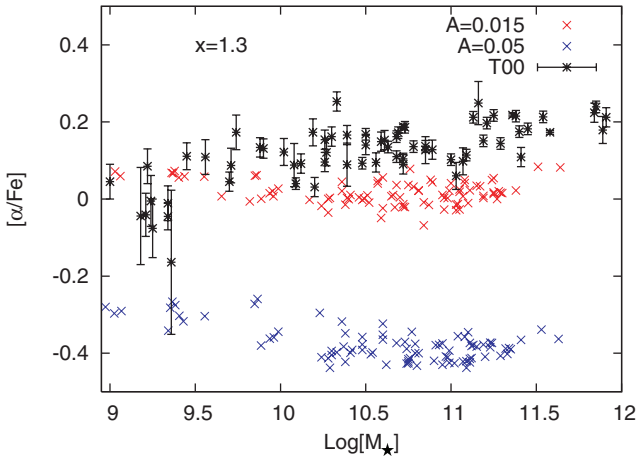

Figure 9. Relation between the [α/Fe] ratio and stellar mass. Symbols – red crosses: SAM+GCE with $x = 1.3$ and $A = 0.015$; blue crosses: SAM+GCE with $x = 1.3$ and $A = 0.05$; black stars with error bars: galaxies from Trager et al. (2000a), re-analysed as discussed in the text. Note again the poor agreement of the model galaxies with the observations.

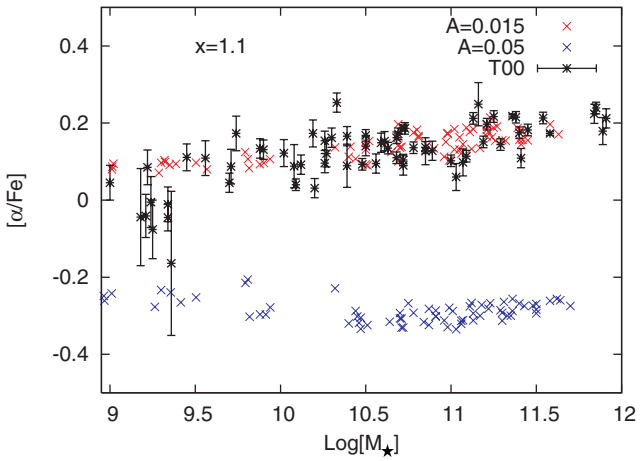

Figure 10. As in Fig. 9, except $x = 1.1$ for the model galaxies from the SAM+GCE. Note the better agreement with observations when using a low value of the SN Ia fraction A.

forming stars in a regime of enhanced [α/Fe] (higher metallicity yields).

In summary, we had expected that the inclusion of AGN feedback in the SAMs might solve the problems that previous studies have encountered in trying to reproduce the observed trend between mass and [α/Fe] ratio, because the quenching due to AGN does lead to more massive galaxies having shorter formation time-scales in the models. However, apparently the effect of 'downsizing' on the trend of [α/Fe] is very small and a flatter IMF is required to achieve agreement between the models and the observations. This does not undermine the potential importance of AGN feedback, which appears to be a promising mechanism for solving many of the other problems experienced by earlier generations of models (such as the overcooling problem). In any case, it is encouraging that with minor variations (within the observational uncertainties) in the chemical evolution parameters, we can for the first time obtain very good agreement with the observed mass–[α/Fe] in a SAM.

One concern is that the comparison between our models and the observations is not strictly rigorous since we are showing

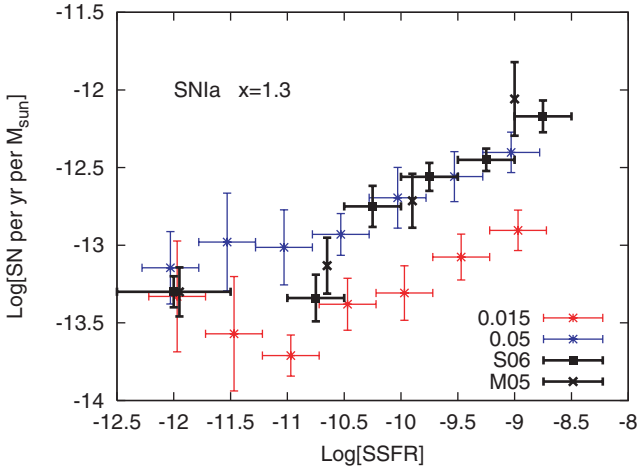

Figure 11. Present day SN Ia rate as a function of SSFR. Here we show all model galaxies, regardless of morphology. Red stars are SAM+GCE with $x = 1.3$ and $A = 0.015$; blue stars are SAM+GCE with $x = 1.3$ and $A = 0.05$; black squares are observations from Sullivan et al. (2006) and black crosses from Mannucci et al. (2005). The conversion of galaxy type into SSFR for the Mannucci et al. data points is the same as in Sullivan et al. (2006).

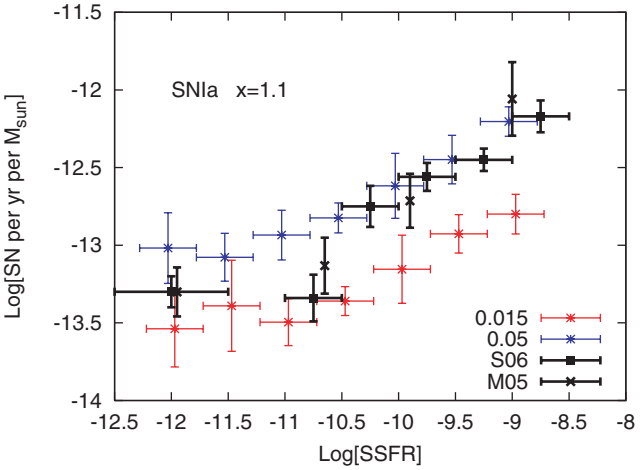

Figure 12. As in Fig. 11, except using the shallower IMF ($x = 1.1$) for the model galaxies from the SAM+GCE.

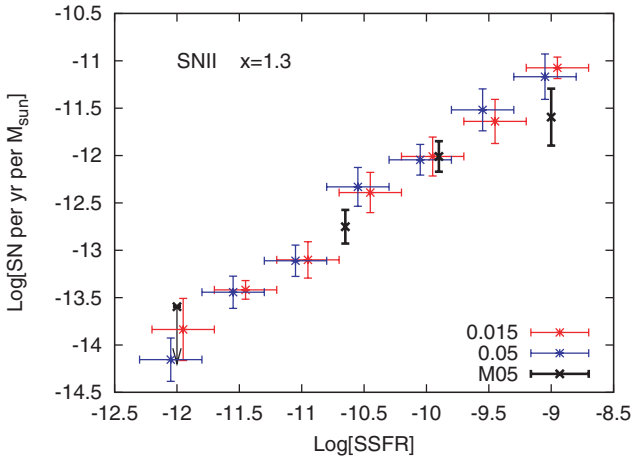

Figure 13. Present-day SN II rate as a function of SSFR. Symbols are as in Fig. 11. Results are shown for the standard IMF ($x = 1.3$). We remind the reader that the upper-mass limit on the IMF is $40\,M_{\odot}$.

stellar mass-weighted abundances for the models, while stellar population studies derive abundances from line-strength indexes from integrated spectra, which are themselves light-weighted quantities. However, TS09 have shown that the SSP-equivalent (absorption-line-weighted) metallicity correlates very well with its mass-weighted and light-weighted counterparts. In future work, nevertheless, we will synthesize line strengths for the galaxies in our simulations and calculate abundance ratios in the same way as is done in the observational data. One additional worry is the effect of limited aperture size on the comparison, as early-type galaxies are well known to have significant line-strength gradients. These gradients imply however mild *metallicity* gradients but *no abundance ratio* gradients whatsoever (e.g. Davies, Sadler & Peletier 1993; Mehlert et al. 2003; Sánchez-Blázquez et al. 2007; TS09). Therefore, we are confident that trends in $[\alpha/\mathrm{Fe}]$ with mass are trustworthy. We note here (as described in Appendix B) that the data plotted in the figures have been constructed to appear as if the galaxies were at the distance of the Coma cluster and observed through fibre apertures of diameter 2.7 arcsec (see Trager et al. 2008). While this does not eliminate gradient effects on the inferred metallicities, it reduces their magnitude to an offset of roughly -0.1 dex (TS09).

SNe rates provide further independent constraints our models. We calculate the predicted SNe rates for our model galaxies and compare them with those derived by Mannucci et al. (2005) and Sullivan et al. (2006) for a large sample of galaxies in the nearby Universe. In Figs 11 and 12 we show the present day SN Ia rate in units of SN events per year per unit stellar mass versus the specific star formation rate (SSFR, SFR per unit stellar mass), and in Figs 13 and 14 we show the rates for SNe II. Here we show all the model galaxies regardless of morphology, since the early-type galaxies populate only the lower SSFR side of these diagrams, and both comparison samples include galaxies of all morphological types. The galaxies in these samples are from a mixture of field and small cluster environments, but so are our model galaxies.

The slope of the IMF has little effect on the predicted SN Ia rates; only the A parameter has a significant influence on the results. From Figs 11 and 12, we see that no combination of IMF slope and fraction of binaries that yield SNe Ia can fit the observations over the whole range of SSFR. However, it is interesting to notice that SNe Ia rates of star-forming galaxies (SSFR $> 10^{-10.5}$) are very well matched by models with a high value of A, while a low value of A is a better match for passive galaxies (SSFR $< 10^{-10.5}$). This behaviour, which is seen regardless of the slope of the IMF, is almost certainly due to the chosen SN Ia model. In the Greggio & Renzini (1983) formalism which we use, the DTD of the SN Ia explosions is given by a convolution of the distribution of secondary masses (in binary systems) and the lifetime of the secondary star. On the other hand, from the same observational data, Mannucci et al. (2006) derived a DTD with two components: a prompt peak and a later plateau, each encompassing half of the SNe Ia. Other authors have also reached similar conclusions about the DTD of Type Ia explosions (e.g. Scannapieco & Bildsten 2005; Dahlen, Strolger & Riess 2008). This bimodal DTD effectively enhances the production of SNe Ia in star-forming galaxies, exactly where a higher fraction of SN Ia are needed in our models. We therefore expect that using a two-population DTD with a significant prompt component will

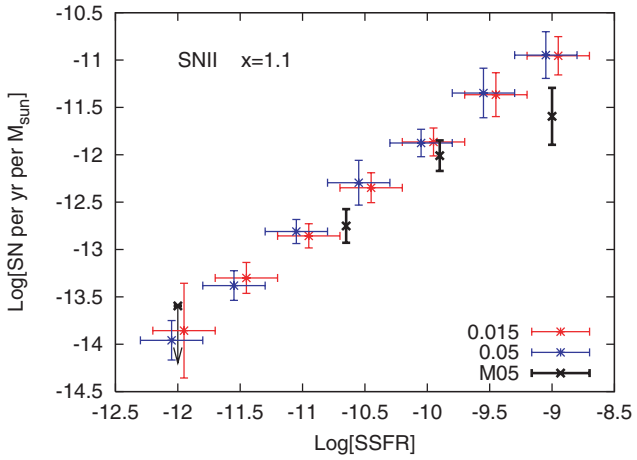

Figure 14. The same as Fig. 13, except we use the shallower IMF slope ($x = 1.1$) for the model galaxies from the SAM+GCE.

alleviate the differences between our model predictions and the observed Type Ia rates, and we show that this is the case below.

The SN II rates, on the other hand, show very good agreement with the observations over the whole range of SSFR. In this case, all variations of x and A give the same qualitative results, although the models with the 'standard' parameter values are slightly better. Nevertheless, as we have shown above, not all combinations of IMF slopes and values of A (SN Ia producing fraction of binaries) produce model galaxies that agree with observed metallicities and abundance ratios. It is only for those models with a shallower IMF ($x \sim 1.1$) and lower SNe Ia fraction among binaries ($A \sim 0.01$–0.02) that we can reasonably reproduce the full set of observations.

To summarize, after implementing detailed chemical evolution in the SAM of S08, we can now reproduce the mass–metallicity and mass–[α/Fe] relations for local early-type galaxies, provided we use a slightly flatter Chabrier IMF and a low fraction of binaries giving rise to SN Ia. The predicted rates of SNe Ia show a strong dependence on the fraction of binaries that yield such an event (our parameter A) but not on the slope of the IMF, with the rates in star-forming galaxies better matched by a high value of A, while those in passive galaxies are better with a low value of A. However, for a standard IMF and high value of A, the galaxies are a bit too metal poor and, most importantly, the abundance ratios are extremely low, in severe disagreement with observations.

4.2.2 *Bimodal delay time distribution for SNe Ia*

In the previous section, we speculated that a bimodal distribution with a prompt population of SNe Ia explosions would give a better match for the observed SN rates. Given the analytical nature of the DTD formulation (Greggio 2005), it is fairly straightforward to implement and test this hypothesis. We have implemented the DTD proposed by Mannucci et al. (2006). Fig. 15 shows the four observational constraints used to test the models (metallicity versus stellar mass, [α/Fe] versus stellar mass, Type Ia supernova remnant (SNR) versus SSFR and Type II SNR versus SSFR). Clearly the new double-peaked SN Ia DTD model gives a better match to the SN Ia rates, while maintaining the good agreement in the other galactic

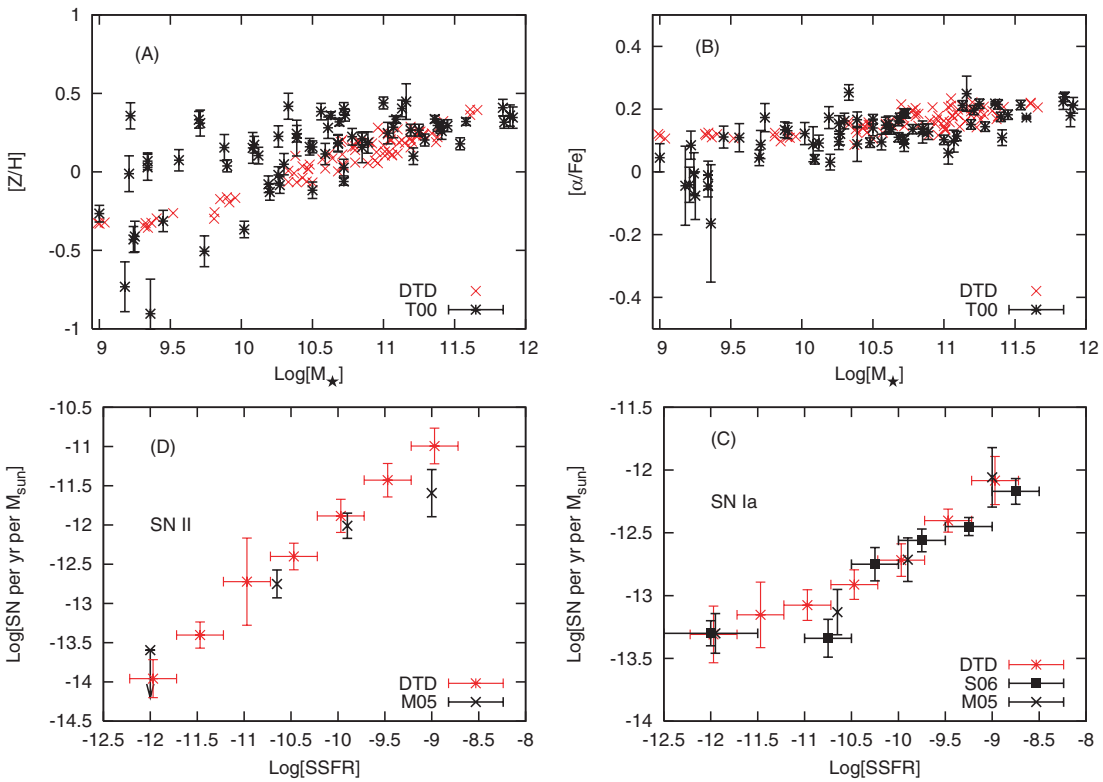

Figure 15. Clockwise, starting from the top left-hand panel: (A) [Z/H] versus stellar mass; (B) [α/Fe] versus stellar mass; (C) Type Ia SNR versus SSFR; (D) Type II SNR versus SSFR. Symbols – red crosses: SAM+GCE with bimodal DTD for SNe Ia ($x = 1.15$, $A = 0.03$); T00: re-analysed metallicities and abundance ratios from Trager et al. (2000a); M05 and S06: SN rates from Mannucci et al. (2005) and Sullivan et al. (2006), respectively.

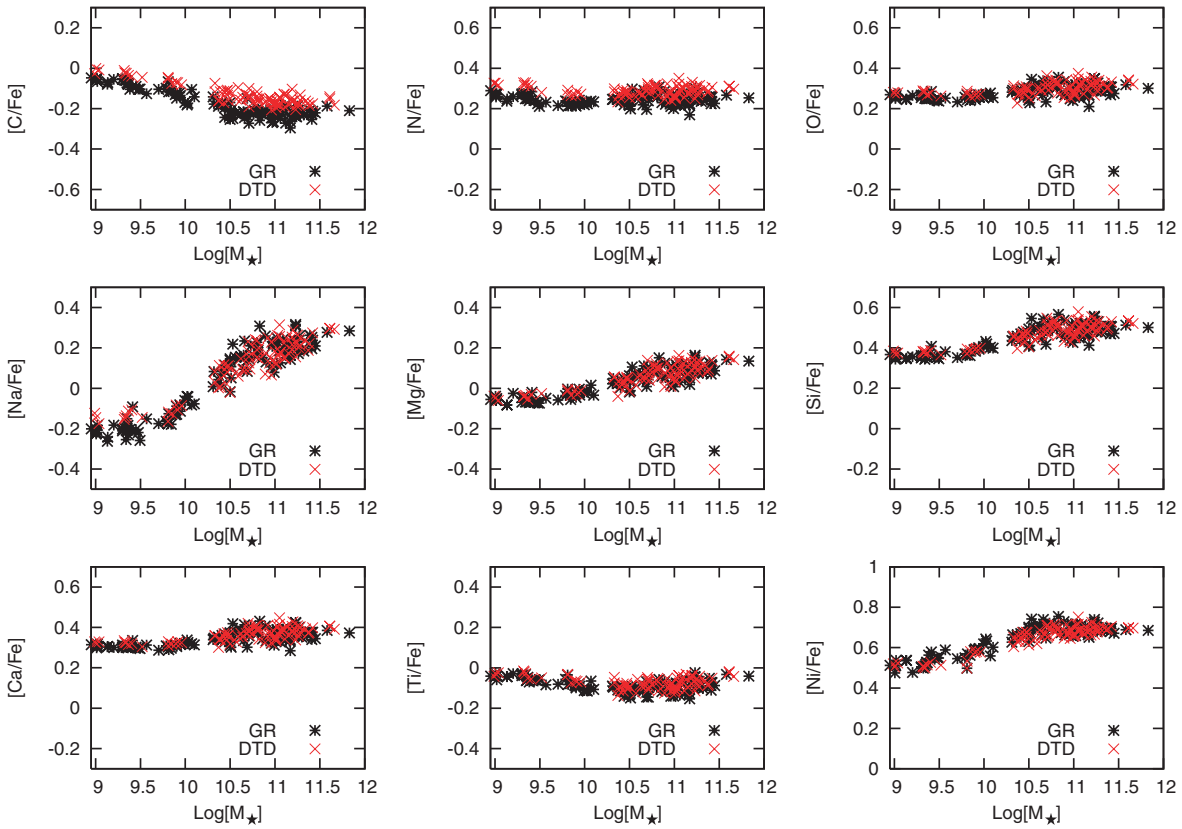

Figure 16. Elemental abundance ratios versus stellar mass for some α-elements and Fe-peak elements. Only predictions from our best-fitting models are shown. Symbols – black stars: classic SN Ia (Greggio & Renzini 1983); red crosses: DTD formulation (Greggio 2005). The parameters are ($x = 1.1, A = 0.015$) and ($x = 1.15, A = 0.03$), respectively.

properties. However, for this model, the best-fitting parameters for the IMF slope and the SN Ia binary fraction are slightly different; specifically, $x = 1.15$ and $A = 0.03$. This value for the IMF is in even better agreement with some recent studies (Baldry & Glazebrook 2003; Wilkins et al. 2008) than our previous 'best' value of $x = 1.1$.

Finally, in Fig. 16 we show the abundance ratios of some individual elements for the galaxies in our best-fitting models using the classic SNe Ia recipe ($x = 1.1$ and $A = 0.015$) and the bimodal DTD ($x = 1.15$ and $A = 0.03$). With the exception of C and N, which are slightly higher for the latter, all the elements follow the same trends in both models. In particular Mg, even though it is underabundant with respect to other α-elements, is the one element that best follows the observed trend of [α/Fe]. This leads us to believe that the abundances derived from the stellar population analysis may be predominantly driven by Mg, and may not necessarily reflect of all the α-elements. There is also an excess of Ni in the Fe-peak group and a decreasing trend of [C/Fe] with increasing galactic mass which is apparently not observed (Sánchez-Blázquez et al. 2003; Graves & Schiavon 2008). This should not be considered a flaw of the model, since the abundances of individual elements are very sensitive to the chosen yields. We expect that future line-strength observations, interpreted with next-generation stellar population models (such as Schiavon 2007; Lee et al. 2009), will provide an interesting test of our models, including the set of assumed yields (WW95; N97; KL07).

4.2.3 Dependence on other model parameters

We have also explored whether we could match the observations investigated above by varying the galaxy formation parameters of the SAM instead of the IMF and binary fraction parameters. For this purpose, we ran several simulations in which we modified the star formation efficiency (A_K in equation 2), the SN feedback efficiency ($\epsilon_0^{\rm SN}$ in equation 3) and the virial velocity below which ejection of reheated gas from the halo into the diffuse IGM becomes important ($V_{\rm eject}$ in equation 4). When the star formation efficiency was increased by a constant factor, a few more massive galaxies were produced and the slope of the mass–[α/Fe] relation increased slightly but the slope and zero-point of the mass–metallicity relation did not change. A higher SF efficiency implies that the cold gas is consumed more rapidly and therefore the time-scale for star formation is shorter, which is why the mass–[α/Fe] relation was affected.

If A_K was allowed to increase with increasing galactic baryonic mass, a considerable number of very massive galaxies were produced and the slope of the mass–metallicity relation increased mildly (but not the zero-point). On the other hand, if the factor decreased with increasing galactic mass, the trends remained the same but no galaxies above 10^{11} M$_\odot$ were produced. This excess or lack of high-mass galaxies arises because star formation in the biggest systems is either boosted or suppressed by this mass-dependent variation of the star formation efficiency.

The effects of reducing the SN feedback efficiency and the $V_{\rm eject}$ parameter were roughly the same. In both cases the slope and zero-point of the mass–metallicity relation increased slightly and the central galaxies of the DM haloes were on average more massive, but the mass–[α/Fe] relation did not change and an unrealistically large number of low-mass satellite galaxies was also produced. This excess of low-mass satellites is due to the fact that small galaxies retain their gas more efficiently when these parameters that control the SN feedback are decreased.

Overall, the effect of changing these other parameters is not as strong as flattening the IMF, and also destroys the agreement with other well-calibrated observations, such as the luminosity function, the metallicity distribution function and the cold gas fraction. We therefore conclude that our results are robust to the values of these free parameters.

As a final test, we modified some of the yields. Specifically, we decreased the Fe yield of SNe II by half and increased the Mg yield by a factor of 4. Reducing the Fe yield had very little effect, indicating that the bulk of the Fe comes from SNe Ia, as expected. Changing the Mg yield raised the zero-point of the relations, as expected. However, neither of these changes affected the slope. Pipino et al. (2009) reached a similar conclusion about the yields and other parameters when exploring the parameter space in their models.

5 DISCUSSION AND CONCLUSIONS

We have implemented detailed GCE in a SAM, and use the resulting model to study the metal enrichment of early-type galaxies in the local Universe. The base SAM is that presented in S08. We take into account the effects of galaxy mergers, inflow of cold gas, and SN and AGN-driven outflows, as well as the production of metals by SN Ia, SN II and AGB stars. Unlike most previous SAMs we discard the instantaneous recycling approximation by properly accounting for the finite lifetimes of the stars and also make use of metallicity-dependent yields.

We run our SAM+GCE simulations in a grid of DM haloes ranging over present-day masses of 10^{11} to $10^{13}\,{\rm M}_{\odot}$. We allow the slope of the IMF and the fraction of binaries that produce a SN Ia event to vary, and compare our results with the observed trends of metallicity and abundance ratio ([α/Fe]) against stellar mass of the galaxies, as well as the SN rate (both Type Ia and II) as a function of SSFR. Only the models with a shallow IMF ($x = 1.1$) and a low fraction of SN Ia from binaries ($A \sim 0.015$) match all four observations of early-type galaxies simultaneously. A slightly flatter than standard IMF is necessary in order to produce more massive stars, which enrich the ISM more efficiently, making the galaxies in our simulations become more metal rich and improving the agreement with the data. The production of more massive stars, along with the fact that the SFHs are more extended in time as the galaxy mass decreases, helps to achieve the correct trend of increasing [α/Fe] with increasing galaxy stellar mass. However, it is also necessary to invoke a low fraction of SNe Ia to raise the zero-point of this relation. We also predict abundance patterns for a variety of elements for early-type galaxies at $z = 0$ in our fiducial model. These predictions will be interesting to compare with future observations.

From studying the SNe Ia rates, we find evidence supporting a 'two-population' distribution for the Type Ia explosions, since galaxies with high SSFRs are better matched by models with a high fraction of binaries that explode as SN Ia (A) while those with low SSFR require a low value of A. We tested whether the use of a more realistic (bimodal) DTD of SNe Ia would, in fact, improve the results. After implementing the DTD formulation for SNe Ia and using a bimodal distribution with a prompt peak and an extended plateau, we found very good agreement with the SN rates, while still matching the trends of [Z/H] and [α/Fe] with stellar mass, although the best values for the slope of the IMF changed slightly and the fraction of SNe Ia binaries needed to be doubled. Our favoured model is now one with a Chabrier-like IMF with a slope of $x = 1.15$, a SNe Ia binary fraction of $A = 0.03$ (relative to the 3–16 $\rm M_{\odot}$ range, $A \sim 0.0014$ relative to the full range of masses defining the IMF) and a bimodal DTD for SN Ia events as proposed by Mannucci et al. (2006).

We have also studied the effects of varying the galaxy formation parameters in the SAM, but found that we were unable to reproduce the observations in this way. We therefore conclude that our results are robust to the values of the free parameters in the SAM.

This is not the first time that a GCE model has been applied within a SAM. Nagashima et al. (2005a,b) have also constructed such a model, and their 'superwind' model resembles our model. They first obtained fairly good agreement with observations of ICM abundances in galaxy clusters, however, the same models failed to reproduced the trend of increasing [α/Fe] with increasing galactic mass. One of the main differences between their models and ours is in fact the IMF. They use a Kennicutt IMF ($x = 1.5$) for quiescent star formation and a flat IMF ($x = 0.0$) for stars formed in bursts. This flat IMF is rather extreme, while the proposed modification in our models is small, in fact within the observational uncertainties. Namely, we require the same 'shallow' IMF ($x = 1.15$) for all modes of star formation. Another model that reproduces the observed scaling of abundance ratio with galaxy mass is that of Pipino & Matteucci (2004, 2006). However, they consider a very different scenario for galaxy formation, the monolithic collapse scenario, and allow for galaxy mergers only in the form of a second infalling episode. More recently, Pipino et al. (2009) also coupled GCE to a SAM, but they also failed to match the mass–[α/Fe] relation. They claim that flattening the IMF cannot solve this problem, in contradiction with our findings. It is worth mentioning that none of these models includes AGN feedback; only the GalICS model used by Pipino et al. (2009) has some form of halo quenching simply by shutting down the flow of cold gas on to galaxies with masses larger than $10^{11}\,{\rm M}_{\odot}$. However, contrary to our expectations, we find that star formation quenching by AGN is not a key factor in our success at reproducing the mass–[α/Fe] relation, even though the AGN feedback in our models leads to shorter formation times for the more massive galaxies. We find that a slight flattening of the IMF is essential to achieve agreement between the model and the observations. AGN feedback, nonetheless, is likely to play an important role in reproducing other galaxy observations, such as the stellar mass or luminosity function and colour bimodality.

Our best-fitting IMF, nonetheless, is consistent with observations; the slope is within the observational uncertainty of Chabrier (2003) and agrees remarkably well with the results of Baldry & Glazebrook (2003), who found that ultraviolet to near-infrared galaxy luminosity densities require an IMF with a slope of 1.15 ± 0.2. The same slope was found by Wilkins et al. (2008) when trying to reconcile the redshift evolution of the observed stellar mass density with the cosmic SFH using a constant and universal IMF. The agreement, however, holds only at low redshift. In a forthcoming paper, Wilkins et al. (in preparation) propose an evolving IMF as a plausible solution. Such an IMF should be strongly top-heavy

at high redshift (Hopkins, private communication). van Dokkum (2008) also suggests an evolving Chabrier-like IMF based on comparing the evolution of the M/L ratios of early-type galaxies to their colour evolution, but in this case the change is in the characteristic mass (m_c in equation 11) rather than the slope, making the IMF 'bottom light' at high redshift. Such evolving IMFs could, in principle, work in favour of the trends of [α/Fe] with stellar mass and SNR with SSFR since they produce either more SN II or fewer SN Ia progenitors at earlier times when massive early-type galaxies create most of their stars. This scenario remains to be tested, and moreover the issue of an evolving IMF is open to considerable debate given the large uncertainties on its constraints. On a different note, Meurer et al. (2009) has claimed evidence for an IMF that depends on galactic surface brightness (or surface density) as a plausible explanation for an observed variation in H α/FUV flux ratio. However, they invoke variations that are an order of magnitude larger than the deviation of our best-fitting slope from the standard value. Finally, very recently, Calura & Menci (2009) have claimed that a constant IMF cannot account for the trends of [Z/H] and [α/Fe] with velocity dispersion in elliptical galaxies and have proposed an IMF with a slope depending on the SFR ($x = 1.35$ for low star-forming systems and $x = 1$ for high star-forming systems) in order to explain them. However, their chemical evolution is not coupled to a SAM, but is computed a posteriori with SFHs extracted from the SAM of Menci et al. (2008), and therefore the flows of enriched gas from the galaxies into the haloes and back again are not tracked, unlike in the our model.

In future work we will apply this model to other questions such as the abundances of different components of spiral galaxies like the Milky Way (e.g. the disc, bulge and stellar halo), abundances in clusters versus the field, abundances in the intracluster gas and to the evolution of metals over cosmic time.

ACKNOWLEDGMENTS

We thank the directors of the Max-Planck-Institut für Astronomie, H.-W. Rix, and the Kapteyn Astronomical Institute, J. M. van der Hulst, and NOVA, the Lorentz Center and the Leids Kerkhoven-Bosscha Fonds for providing travel support and working space during the gestation of this paper. BKG acknowledges the support of the UK's Science & Technology Facilities Council (STFC Grant ST/F002432/1) and the Commonwealth Cosmology Initiative. We also thank Francesca Matteucci for helpful advice at an early stage of this project, and the anonymous referee for insightful questions and comments.

REFERENCES

Baldry I. K., Glazebrook K., 2003, ApJ, 593, 258
Baldry I. K., Glazebrook K., Brinkmann J., Ivezić Ž., Lupton R. H., Nichol R. C., Szalay A. S., 2004, ApJ, 600, 681
Baugh C. M., Lacey C. G., Frenk C. S., Granato G. L., Silva L., Bressan A., Benson A. J., Cole S., 2005, MNRAS, 356, 1191
Bell E. F., McIntosh D. H., Katz N., Weinberg M. D., 2003, ApJ, 585, L117
Benson A. J., Bower R. G., Frenk C. S., Lacey C. G., Baugh C. M., Cole S., 2003, ApJ, 599, 38
Bertelli G., Bressan A., Chiosi C., Fagotto F., Nasi E., 1994, A&AS, 106, 275
Bower R. G., Benson A. J., Malbon R., Helly J. C., Frenk C. S., Baugh C. M., Cole S., Lacey C. G., 2006, MNRAS, 370, 645
Boylan-Kolchin M., Ma C.-P., Quataert E., 2008, MNRAS, 383, 93
Bruzual G., Charlot S., 2003, MNRAS, 344, 1000
Calura F., Menci N., 2009, MNRAS, in press (arXiv:0907.3729)
Cappellari M. et al., 2006, MNRAS, 366, 1126
Cardelli J., Clayton G., Mathis J., 1989, ApJ, 345, 245
Cattaneo A., Dekel A., Devriendt J., Guiderdoni B., Blaizot J., 2006, MNRAS, 370, 1651
Chabrier G., 2001, ApJ, 554, 1274
Chabrier G., 2003, PASP, 115, 763
Charlot S., Fall S. M., 2000, ApJ, 539, 718
Cole S., Aragón-Salamanca A., Frenk C. S., Navarro J. F., Zepf S. E., 1994, MNRAS, 271, 781
Cole S., Lacey C. G., Baugh C. M., Frenk C. S., 2000, MNRAS, 319, 168
Cox T. J., Jonsson P., Somerville R. S., Primack J. R., Dekel A., 2008, MNRAS, 384, 386
Croton D. J. et al., 2006, MNRAS, 365, 11
Dahlen T., Strolger L.-G., Riess A. G., 2008, ApJ, 681, 462
Davies R. L., Sadler E. M., Peletier R. F., 1993, MNRAS, 262, 650
De Lucia G., Kauffmann G., White S. D. M., 2004, MNRAS, 349, 1101
De Lucia G., Springel V., White S. D. M., Croton D., Kauffmann G., 2006, MNRAS, 366, 499
de Plaa J., Werner N., Bleeker J. A. M., Vink J., Kaastra J. S., Méndez M., 2007, A&A, 465, 345
Fenner Y., Gibson B. K., 2003, Publ. Astron. Soc. Australia, 20, 189
Fontanot F., De Lucia G., Monaco P., Somerville R. S., Santini P., 2009, MNRAS, 397, 1776
François P., Matteucci F., Cayrel R., Spite M., Spite F., Chiappini C., 2004, A&A, 421, 613
Gibson B. K., Matteucci F., 1997, MNRAS, 291, L8
Gnedin N. Y., 2000, ApJ, 542, 535
Graves G. J., Schiavon R. P., 2008, ApJS, 177, 446
Greggio L., 2005, A&A, 441, 1055
Greggio L., Renzini A., 1983, A&A, 118, 217
Grevesse N., Noels A., Sauval A. J., 1996, in Holt S. S., Sonneborn G., eds, ASP Conf. Ser. Vol. 99, Cosmic Abundances. Astron. Soc. Pac., San Francisco, p. 117
Hatton S., Devriendt J. E. G., Ninin S., Bouchet F. R., Guiderdoni B., Vibert D., 2003, MNRAS, 343, 75
Kang X., Jing Y. P., Mo H. J., Börner G., 2005, ApJ, 631, 21
Kannappan S. J., 2004, ApJ, 611, L89
Karakas A., Lattanzio J. C., 2007, Publ. Astron. Soc. Australia, 24, 103 (KL07)
Kauffmann G., White S. D. M., Guiderdoni B., 1993, MNRAS, 264, 201
Kennicutt R. C., Jr, 1989, ApJ, 344, 685
Kimm T. et al., 2009, MNRAS, 394, 1131
Komatsu E. et al., 2009, ApJS, 180, 330
Korn A. J., Maraston C., Thomas D., 2005, A&A, 438, 685
Kravtsov A. V., Gnedin O. Y., Klypin A. A., 2004, ApJ, 609, 482
Kroupa P., Tout C. A., Gilmore G., 1993, MNRAS, 262, 545
Lee H.-c. et al., 2009, ApJ, 694, 902
Mannucci F., Della Valle M., Panagia N., Cappellaro E., Cresci G., Maiolino R., Petrosian A., Turatto M., 2005, A&A, 433, 807
Mannucci F., Della Valle M., Panagia N., 2006, MNRAS, 370, 773
Matteucci F., Gibson B. K., 1995, A&A, 304, 11
Matteucci F., Greggio L., 1986, A&A, 154, 279
Matteucci F., Panagia N., Pipino A., Mannucci F., Recchi S., Della Valle M., 2006, MNRAS, 372, 265
Mehlert D., Thomas D., Saglia R. P., Bender R., Wegner G., 2003, A&A, 407, 423
Menci N., Rosati P., Gobat R., Strazzullo V., Rettura A., Mei S., Demarco R., 2008, MNRAS, 685, 863
Meurer G. R. et al., 2009, ApJ, 695, 765
Moster B. P., Somerville R. S., Maulbetsch C., van den Bosch F. C., Maccio' A. V., Naab T., Oser L., 2009, preprint (arXiv:0903.4682)
Nagashima M., Lacey C. G., Baugh C. M., Frenk C. S., Cole S., 2005a, MNRAS, 358, 1247
Nagashima M., Lacey C. G., Okamoto T., Baugh C. M., Frenk C. S., Cole S., 2005b, MNRAS, 363, L31

Nomoto K., Iwamoto K., Nakasato N., Thielemann F.-K., Brachwitz F., Tsujimoto T., Kubo Y., Kishimoto N., 1997, Nuclear Phys. A, 621, 467 (N97)
Pagel B. E. J., 1997, Nucleosynthesis and Chemical Evolution of Galaxies. Cambridge Univ. Press, Cambridge
Pipino A., Matteucci F., 2004, MNRAS, 347, 968
Pipino A., Matteucci F., 2006, MNRAS, 365, 1114
Pipino A., Devriendt J. E. G., Thomas D., Silk J., Kaviraj S., 2009, A&A, 505, 1075
Robertson B., Cox T. J., Hernquist L., Franx M., Hopkins P. F., Martini P., Springel V., 2006, ApJ, 641, 21
Romano D., Chiappini C., Matteucci F., Tosi M., 2005, A&A, 430, 491
Salpeter E. E., 1955, ApJ, 121, 161
Sánchez-Blázquez P., Gorgas J., Cardiel N., Cenarro J., González J. J., 2003, ApJ, 590, L91
Sánchez-Blázquez P., Forbes D. A., Strader J., Brodie J., Proctor R., 2007, MNRAS, 377, 759
Scannapieco E., Bildsten L., 2005, ApJ, 629, L85
Schiavon R. P., 2007, ApJS, 171, 146
Simien F., de Vaucouleurs G., 1986, ApJ, 302, 564
Somerville R. S., Kolatt T. S., 1999, MNRAS, 305, 1
Somerville R. S., Primack J. R., 1999, MNRAS, 310, 1087
Somerville R. S., Primack J. R., Faber S. M., 2001, MNRAS, 320, 504
Somerville R. S. et al., 2008a, ApJ, 672, 776
Somerville R. S., Hopkins P. F., Cox T. J., Robertson B., Hernquist L., 2008b, MNRAS, 391, 481 (S08)
Spergel D. N. et al., 2007, ApJS, 170, 377
Sullivan M. et al., 2006, ApJ, 648, 868
Sutherland R. S., Dopita M. A., 1993, ApJS, 88, 253
Thomas D., 1999, MNRAS, 306, 655
Thomas D., Kauffmann G., 1999, in Hubeny I., Heap S., Cornett R., eds, ASP Conf. Ser. Vol. 192, Spectrophotometric Dating of Stars and Galaxies. Astron. Soc. Pac., San Francisco, p. 261
Thomas D., Greggio L., Bender R., 1999, MNRAS, 302, 537
Thomas D., Maraston C., Bender R., Mendes de Oliveira C., 2005, ApJ, 621, 673
Timmes F. X., Woosley S. E., Weaver T. A., 1995, ApJS, 98, 617
Tinsley B. M., 1980, Fundamentals Cosmic Phys., 5, 287
Trager S. C., Somerville R. S., 2009, MNRAS, 395, 608
Trager S. C., Faber S. M., Worthey G., González J. J., 2000a, AJ, 119, 1645
Trager S. C., Faber S. M., Worthey G., González J. J., 2000b, AJ, 120, 165
Trager S. C., Faber S. M., Dressler A., 2008, MNRAS, 386, 715
Tripicco M. J., Bell R. A., 1995, AJ, 110, 3035
van Dokkum P. G., 2008, ApJ, 674, 29
Wang L., Li C., Kauffmann G., De Lucia G., 2006, MNRAS, 371, 537
White S. D. M., Frenk C. S., 1991, ApJ, 379, 52
White S. D. M., Rees M. J., 1978, MNRAS, 183, 341
Wilkins S. M., Hopkins A. M., Trentham N., Tojeiro R., 2008, MNRAS, 391, 363
Woosley S. E., Weaver T. A., 1995, ApJS, 101, 181 (WW95)
Worthey G., Faber S. M., Gonzalez J. J., 1992, ApJ, 398, 69

APPENDIX A: IMPLEMENTATION ALGORITHM OF THE GCE MODELLING

To compute the chemical enrichment consistently as described in Section 2, it is imperative to keep track of the SFH of each galaxies as well as the metallicity of the ISM as a function of time in these galaxies. Given the large number of galaxies in the simulations, it is very expensive, both in computing time and in physical memory, to store these quantities in a linear time grid with reasonable resolution. In order to overcome these limitations, we use an age grid where first bin of this grid represents $t = t_{\rm now}$ at any moment during the calculations and the size (in time) of the bins increase as we go to older ages. The scaling of the bins is related to the lifetimes of the stars, so that it increases as the lifetimes of the stars become progressively larger. The size of the bins only increases, but each subsequent bin is not necessarily larger than the previous one. In Table A1 we show the structure of this binning grid. In this grid we store the amount of cold gas mass turned into stars, $\Delta M_\star$, and the metallicity of the cold gas, $Z_{\rm g}$. [3] As the systems evolve this information is 'pushed down' to older bins, directly if the subsequent bin is of the same size or added if the bin is of a larger size. In the later case, the cold gas masses are added directly whereas the metallicity is averaged, weighted by the size of the bins. In essence, what we extract from this grid are time-averaged quantities.

Table A1. Structure of the grid where the star formation and abundance histories are stored. All quantities are in Gyr.

Age range	Size of bins
0.00–0.12	0.01
0.12–0.40	0.02
0.40–1.12	0.04
1.12–2.72	0.08
2.72–11.68	0.32
11.68–	1.28

Note. The initial size of the bins is 0.01 Gyr because it is the maximum possible value of the time-step in our simulations.

It is also important how we handle this information when galaxies merge, that is, how we combine the star formation and metallicity histories of the merging galaxies. This is done on a bin-by-bin basis. At a given age bin, $\Delta M_\star$ is added directly and the metallicities are averaged weighted by the corresponding $\Delta M_\star$. In mathematical form

$$\Delta M_\star[i] = \Delta M_\star^{\rm A}[i] + \Delta M_\star^{\rm B}[i], \tag{A1}$$

$$Z_{\rm g} = \frac{Z_{\rm g}^{\rm A} * \Delta M_\star^{\rm A}[i] + Z_{\rm g}^{\rm B} \Delta M_\star^{\rm B}[i]}{\Delta M_\star^{\rm A}[i] + \Delta M_\star^{\rm B}[i]}, \tag{A2}$$

where A and B are the merging galaxies and i the age bin. Summarizing, the SFR and the cold gas metallicity used in equation (9) to calculate the enrichment of the ISM are average quantities.

APPENDIX B: GALAXY SAMPLE

The sample of galaxies used to test our models was taken from Trager et al. (2000a) and re-analysed with the method described in Trager et al. (2008). Specifically, we used the Bruzual & Charlot (2003) stellar population models and modified the line strengths when $[\alpha/{\rm Fe}] \neq 0$ using 'response functions' that have been calculated for each star in each isochrone, a significant improvement over previous methods (e.g. Tripicco & Bell 1995; Korn, Maraston & Thomas 2005). More details can be found in Trager et al. (2008) and Lee et al. (2009). In Table B1 we present the results from this new stellar population synthesis analysis.

[3] The SFR at the time of interest is computed dividing $\Delta\ M_\star$ by the size of the bin.

Table B1. Velocity dispersions, ages, metallicities, enhancement ratios and dynamical masses of the sample galaxies.

Galaxy	Type	log(σ)	log(Age)	[Z/H]	[E/Fe]	log ($M_{\rm dyn}$)
ESO 358−G06	S0	1.763 ± 0.072	$0.807^{+0.114}_{-0.250}$	$-0.431^{+0.083}_{-0.098}$	$-0.005^{+0.066}_{-0.045}$	9.24 ± 0.43
ESO 358−G25	S0	1.690 ± 0.072	$0.779^{+0.326}_{-0.295}$	$-0.732^{+0.159}_{-0.144}$	$-0.044^{+0.126}_{-0.096}$	9.18 ± 0.39
ESO 358−G50	S0	1.732 ± 0.072	$0.707^{+0.129}_{-0.235}$	$-0.412^{+0.098}_{-0.098}$	$-0.076^{+0.076}_{-0.056}$	9.25 ± 0.48
ESO 358−G59	S0	1.653 ± 0.072	$0.544^{+0.235}_{-0.068}$	$-0.266^{+0.053}_{-0.114}$	$0.045^{+0.045}_{-0.035}$	9.00 ± 0.45
ESO 359−G02	S0	1.763 ± 0.072	$0.603^{+0.159}_{-0.189}$	$-0.904^{+0.220}_{-0.189}$	$-0.164^{+0.187}_{-0.500}$	9.36 ± 0.46
IC 1963	S0	1.763 ± 0.072	$0.397^{+0.114}_{-0.068}$	$0.357^{+0.083}_{-0.098}$	$0.085^{+0.045}_{-0.035}$	9.22 ± 0.50
IC 2006	E	2.134 ± 0.024	$1.126^{+0.098}_{-0.114}$	$0.049^{+0.068}_{-0.083}$	$0.162^{+0.025}_{-0.015}$	10.30 ± 0.33
NGC 0221	E	1.731 ± 0.021	$0.975^{+0.068}_{-0.053}$	$-0.398^{+0.038}_{-0.038}$	$-0.026^{+0.025}_{-0.005}$	8.32 ± 0.28
NGC 0224	E	2.185 ± 0.008	$0.926^{+0.129}_{-0.159}$	$0.281^{+0.068}_{-0.038}$	$0.153^{+0.025}_{-0.005}$	10.61 ± 0.15
NGC 0315	E	2.486 ± 0.005	$0.860^{+0.098}_{-0.083}$	$0.316^{+0.038}_{-0.023}$	$0.239^{+0.015}_{-0.005}$	11.85 ± 0.35
NGC 0507	E	2.445 ± 0.009	$0.601^{+0.129}_{-0.098}$	$0.359^{+0.068}_{-0.053}$	$0.179^{+0.035}_{-0.015}$	11.89 ± 0.34
NGC 0584	E	2.278 ± 0.005	$0.531^{+0.053}_{-0.023}$	$0.318^{+0.023}_{-0.023}$	$0.172^{+0.015}_{-0.005}$	10.69 ± 0.30
NGC 0636	E	2.185 ± 0.007	$0.762^{+0.098}_{-0.068}$	$0.160^{+0.053}_{-0.053}$	$0.093^{+0.015}_{-0.015}$	10.48 ± 0.34
NGC 0720	E	2.381 ± 0.011	$0.653^{+0.326}_{-0.174}$	$0.448^{+0.114}_{-0.083}$	$0.249^{+0.056}_{-0.025}$	11.16 ± 0.27
NGC 0821	E	2.281 ± 0.005	$0.950^{+0.068}_{-0.038}$	$0.210^{+0.038}_{-0.023}$	$0.137^{+0.015}_{-0.005}$	10.85 ± 0.28
NGC 0936	S0	2.258 ± 0.026	$1.110^{+0.098}_{-0.098}$	$-0.084^{+0.053}_{-0.053}$	$0.121^{+0.035}_{-0.015}$	10.27 ± 0.42
NGC 1316	S0	2.344 ± 0.024	$0.510^{+0.038}_{-0.053}$	$0.260^{+0.053}_{-0.038}$	$0.109^{+0.025}_{-0.015}$	11.41 ± 0.22
NGC 1336	E	1.982 ± 0.024	$1.073^{+0.114}_{-0.068}$	$-0.367^{+0.053}_{-0.053}$	$0.122^{+0.035}_{-0.015}$	10.02 ± 0.31
NGC 1339	E	2.199 ± 0.024	$1.146^{+0.098}_{-0.129}$	$-0.079^{+0.053}_{-0.053}$	$0.173^{+0.035}_{-0.015}$	10.19 ± 0.40
NGC 1351	E	2.196 ± 0.024	$1.129^{+0.098}_{-0.083}$	$-0.117^{+0.053}_{-0.038}$	$0.140^{+0.025}_{-0.015}$	10.50 ± 0.31
NGC 1373	E	1.875 ± 0.024	$1.010^{+0.083}_{-0.053}$	$-0.313^{+0.068}_{-0.083}$	$0.111^{+0.035}_{-0.015}$	9.45 ± 0.45
NGC 1374	E	2.267 ± 0.024	$0.931^{+0.083}_{-0.068}$	$0.114^{+0.068}_{-0.114}$	$0.149^{+0.025}_{-0.015}$	10.59 ± 0.31
NGC 1375	S0	1.748 ± 0.072	$0.323^{+0.023}_{-0.023}$	$0.068^{+0.053}_{-0.068}$	$-0.045^{+0.035}_{-0.025}$	9.34 ± 0.40
NGC 1379	E	2.114 ± 0.024	$0.913^{+0.083}_{-0.053}$	$-0.020^{+0.053}_{-0.053}$	$0.154^{+0.025}_{-0.015}$	10.26 ± 0.32
NGC 1380	S0	2.340 ± 0.024	$1.008^{+0.114}_{-0.083}$	$0.157^{+0.098}_{-0.068}$	$0.127^{+0.035}_{-0.015}$	10.85 ± 0.28
NGC 1380A	S0	1.740 ± 0.072	$0.476^{+0.235}_{-0.083}$	$-0.012^{+0.114}_{-0.098}$	$-0.041^{+0.056}_{-0.035}$	9.21 ± 0.40
NGC 1381	S0	2.185 ± 0.024	$0.923^{+0.068}_{-0.038}$	$0.104^{+0.053}_{-0.038}$	$0.092^{+0.025}_{-0.005}$	10.12 ± 0.39
NGC 1399	E	2.574 ± 0.024	$1.026^{+0.083}_{-0.053}$	$0.346^{+0.068}_{-0.038}$	$0.212^{+0.025}_{-0.015}$	11.91 ± 0.21
NGC 1404	E	2.415 ± 0.024	$0.994^{+0.068}_{-0.053}$	$0.187^{+0.068}_{-0.038}$	$0.128^{+0.025}_{-0.005}$	10.89 ± 0.32
NGC 1419	E	2.068 ± 0.024	$1.308^{+0.220}_{-0.220}$	$-0.506^{+0.098}_{-0.189}$	$0.173^{+0.045}_{-0.025}$	9.74 ± 0.45
NGC 1427	E	2.243 ± 0.024	$0.981^{+0.038}_{-0.023}$	$-0.062^{+0.023}_{-0.023}$	$0.104^{+0.015}_{-0.005}$	10.72 ± 0.29
NGC 1453	E	2.475 ± 0.005	$1.008^{+0.053}_{-0.053}$	$0.294^{+0.038}_{-0.023}$	$0.182^{+0.015}_{-0.005}$	11.45 ± 0.39
NGC 1461	S0	2.294 ± 0.011	$0.864^{+0.098}_{-0.098}$	$0.155^{+0.083}_{-0.053}$	$0.134^{+0.025}_{-0.015}$	9.88 ± 0.67
NGC 1600	E	2.508 ± 0.009	$0.822^{+0.189}_{-0.114}$	$0.409^{+0.053}_{-0.023}$	$0.224^{+0.025}_{-0.015}$	11.84 ± 0.36
NGC 1700	E	2.356 ± 0.005	$0.519^{+0.038}_{-0.008}$	$0.335^{+0.023}_{-0.023}$	$0.114^{+0.015}_{-0.005}$	11.09 ± 0.32
NGC 2300	E	2.418 ± 0.006	$0.719^{+0.053}_{-0.144}$	$0.404^{+0.053}_{-0.023}$	$0.212^{+0.015}_{-0.005}$	11.13 ± 0.38
NGC 2560	S0	2.303 ± 0.006	$0.810^{+0.159}_{-0.174}$	$0.226^{+0.068}_{-0.053}$	$0.096^{+0.025}_{-0.015}$	10.26 ± 0.94
NGC 2778	E	2.198 ± 0.007	$0.897^{+0.098}_{-0.174}$	$0.243^{+0.053}_{-0.053}$	$0.166^{+0.025}_{-0.005}$	10.39 ± 0.35
NGC 3115	S0	2.378 ± 0.053	$0.574^{+0.159}_{-0.068}$	$0.384^{+0.053}_{-0.053}$	$0.095^{+0.025}_{-0.025}$	10.56 ± 0.32
NGC 3377	E	1.981 ± 0.009	$0.653^{+0.068}_{-0.098}$	$0.038^{+0.038}_{-0.038}$	$0.131^{+0.025}_{-0.005}$	9.90 ± 0.28
NGC 3379	E	2.291 ± 0.005	$0.969^{+0.038}_{-0.023}$	$0.159^{+0.038}_{-0.023}$	$0.168^{+0.015}_{-0.005}$	10.50 ± 0.28
NGC 3384	S0	2.140 ± 0.031	$0.522^{+0.083}_{-0.053}$	$0.332^{+0.053}_{-0.038}$	$0.045^{+0.025}_{-0.015}$	9.70 ± 0.44
NGC 3412	S0	2.013 ± 0.034	$0.632^{+0.098}_{-0.159}$	$0.029^{+0.083}_{-0.083}$	$-0.011^{+0.045}_{-0.035}$	9.34 ± 0.49
NGC 3585	S0	2.307 ± 0.122	$0.710^{+0.129}_{-0.159}$	$0.247^{+0.068}_{-0.053}$	$0.060^{+0.035}_{-0.015}$	11.03 ± 0.35
NGC 3607	S0	2.332 ± 0.101	$0.720^{+0.189}_{-0.174}$	$0.285^{+0.068}_{-0.068}$	$0.098^{+0.035}_{-0.025}$	11.07 ± 0.33
NGC 3608	E	2.259 ± 0.006	$0.930^{+0.083}_{-0.083}$	$0.224^{+0.053}_{-0.038}$	$0.136^{+0.015}_{-0.005}$	10.78 ± 0.28
NGC 3818	E	2.246 ± 0.007	$0.763^{+0.144}_{-0.068}$	$0.361^{+0.038}_{-0.023}$	$0.186^{+0.015}_{-0.005}$	10.73 ± 0.35
NGC 3941	S0	2.117 ± 0.036	$0.422^{+0.083}_{-0.098}$	$0.311^{+0.083}_{-0.098}$	$0.087^{+0.045}_{-0.035}$	9.71 ± 0.42
NGC 4026	S0	2.258 ± 0.029	$0.542^{+0.159}_{-0.083}$	$0.153^{+0.098}_{-0.083}$	$0.088^{+0.056}_{-0.035}$	10.08 ± 0.41
NGC 4036	S0	2.220 ± 0.039	$0.574^{+0.114}_{-0.129}$	$0.418^{+0.083}_{-0.038}$	$0.253^{+0.025}_{-0.015}$	10.33 ± 0.45
NGC 4111	S0	2.127 ± 0.019	$0.464^{+0.023}_{-0.008}$	$0.074^{+0.068}_{-0.083}$	$0.109^{+0.045}_{-0.035}$	9.56 ± 0.56
NGC 4251	S0	2.072 ± 0.074	$0.514^{+0.038}_{-0.038}$	$0.173^{+0.053}_{-0.038}$	$0.040^{+0.015}_{-0.015}$	10.09 ± 0.38

Table B1 – *continued*

Galaxy	Type	log(σ)	log(Age)	[*Z*/H]	[E/Fe]	log ($M_{\rm dyn}$)
NGC 4261	E	2.479 ± 0.005	$1.136^{+0.053}_{-0.053}$	$0.284^{+0.038}_{-0.023}$	$0.175^{+0.015}_{-0.005}$	11.40 ± 0.28
NGC 4697	E	2.211 ± 0.009	$0.924^{+0.068}_{-0.053}$	$0.027^{+0.053}_{-0.038}$	$0.090^{+0.025}_{-0.005}$	10.72 ± 0.23
NGC 5638	E	2.186 ± 0.006	$0.946^{+0.068}_{-0.038}$	$0.185^{+0.053}_{-0.023}$	$0.162^{+0.015}_{-0.005}$	10.68 ± 0.29
NGC 5812	E	2.300 ± 0.005	$0.602^{+0.235}_{-0.114}$	$0.403^{+0.038}_{-0.098}$	$0.188^{+0.005}_{-0.025}$	10.72 ± 0.33
NGC 5813	E	2.327 ± 0.007	$1.127^{+0.098}_{-0.083}$	$0.100^{+0.053}_{-0.038}$	$0.197^{+0.015}_{-0.005}$	11.21 ± 0.26
NGC 5831	E	2.206 ± 0.004	$0.560^{+0.023}_{-0.023}$	$0.360^{+0.023}_{-0.008}$	$0.135^{+0.015}_{-0.005}$	10.63 ± 0.31
NGC 5846	E	2.354 ± 0.005	$0.980^{+0.068}_{-0.038}$	$0.296^{+0.038}_{-0.023}$	$0.215^{+0.015}_{-0.005}$	11.38 ± 0.23
NGC 5866	S0	2.143 ± 0.116	$0.413^{+0.098}_{-0.098}$	$0.215^{+0.114}_{-0.114}$	$0.089^{+0.056}_{-0.045}$	10.39 ± 0.36
NGC 6127	E	2.393 ± 0.007	$0.981^{+0.053}_{-0.038}$	$0.266^{+0.038}_{-0.023}$	$0.217^{+0.015}_{-0.005}$	11.25 ± 0.41
NGC 6702	E	2.243 ± 0.005	$0.325^{+0.038}_{-0.008}$	$0.439^{+0.038}_{-0.023}$	$0.102^{+0.015}_{-0.015}$	11.00 ± 0.30
NGC 6703	E	2.258 ± 0.006	$0.790^{+0.083}_{-0.068}$	$0.180^{+0.053}_{-0.023}$	$0.110^{+0.015}_{-0.005}$	10.68 ± 0.32
NGC 7052	E	2.464 ± 0.006	$1.218^{+0.068}_{-0.068}$	$0.179^{+0.038}_{-0.038}$	$0.213^{+0.015}_{-0.005}$	11.54 ± 0.38
NGC 7454	E	2.028 ± 0.011	$0.692^{+0.053}_{-0.144}$	$-0.128^{+0.053}_{-0.038}$	$0.031^{+0.025}_{-0.015}$	10.20 ± 0.31
NGC 7562	E	2.391 ± 0.003	$0.924^{+0.023}_{-0.023}$	$0.203^{+0.038}_{-0.008}$	$0.144^{+0.015}_{-0.005}$	11.29 ± 0.35
NGC 7619	E	2.498 ± 0.004	$1.051^{+0.053}_{-0.023}$	$0.320^{+0.023}_{-0.023}$	$0.173^{+0.005}_{-0.005}$	11.58 ± 0.30
NGC 7626	E	2.414 ± 0.004	$0.963^{+0.038}_{-0.023}$	$0.336^{+0.023}_{-0.008}$	$0.218^{+0.005}_{-0.005}$	11.36 ± 0.37
NGC 7785	E	2.378 ± 0.005	$0.911^{+0.068}_{-0.038}$	$0.266^{+0.038}_{-0.008}$	$0.151^{+0.015}_{-0.005}$	11.19 ± 0.39

We also present dynamical mass computed using

$$M_{\rm dyn} = 465\sigma^2 r_{\rm e}, \tag{B1}$$

where σ is the central velocity dispersion in $\mathrm{km\,s^{-1}}$ (here we use the velocity dispersion taken through an aperture of diameter $r_{\rm e}/8$) and $r_{\rm e}$ is effective radius in parsecs (see Trager et al. 2000b, for more details).

This paper has been typeset from a TEX/LATEX file prepared by the author.